FFI RAPPORT

THERMAL AND MECHANICAL ANALYSES FOR THE NSAT-1 PHASE B STUDY

SAGSVEEN Bendik Andreas

FFI/RAPPORT-2003/01407

FFIFv/83401/924

Approved
Kjeller 21. February 2003

Bjørn Bergersen
Assistant Director

THERMAL AND MECHANICAL ANALYSES FOR THE NSAT-1 PHASE B STUDY

SAGSVEEN Bendik Andreas

FFI/RAPPORT-2003/01407

FORSVARETS FORSKNINGSINSTITUTT
Norwegian Defence Research Establishment
P O Box 25, NO-2027 Kjeller, Norway

FORSVARETS FORSKNINGSINSTITUTT (FFI)
Norwegian Defence Research Establishment

P O BOX 25
N0-2027 KJELLER, NORWAY

UNCLASSIFIED

SECURITY CLASSIFICATION OF THIS PAGE (when data entered)

REPORT DOCUMENTATION PAGE

1) PUBL/REPORT NUMBER	2) SECURITY CLASSIFICATION	3) NUMBER OF PAGES
FFI/RAPPORT-2003/01407	UNCLASSIFIED	70
1a) PROJECT REFERENCE	**2a) DECLASSIFICATION/DOWNGRADING SCHEDULE**	
FFIFv/83401/924	-	

4) TITLE

THERMAL AND MECHANICAL ANALYSES FOR THE NSAT-1 PHASE B STUDY

5) NAMES OF AUTHOR(S) IN FULL (surname first)

SAGSVEEN Bendik Andreas

6) DISTRIBUTION STATEMENT

Approved for public release. Distribution unlimited. (Offentlig tilgjengelig)

7) INDEXING TERMS

IN ENGLISH:	IN NORWEGIAN:
a) Satellite	a) Satellitt
b) Finite Element Analyses	b) Finite Element analyser
c) Mechanical design	c) Mekanisk design
d) Thermal design	d) Termisk design
e) Honeycomb	e) Honeycomb

THESAURUS REFERENCE:

8) ABSTRACT

The Norwegian Defence Research Establishment (FFI) and industry partners are looking into a possible development of a micro satellite system (NSAT-1) with an X-band vessel-detector antenna to geolocation vessels for maritime surveillance. To achieve high geolocation accuracy, the pointing direction of the vessel-detector antenna has to be known with an extreme accuracy. A star tracker is mounted to the backside of the antenna panel to determine the exact pointing direction of the antenna.

In this phase B study, it is focused on the antenna panel, the star tracker assembly and the bracket connecting them. The thermal and mechanical requirements set to this system are critical to the concept. Attention is also paid to the loadcases, describing detailed thermal loads both during power generation and observation.

This report reveals the thermal and mechanical analyses for the NSAT-1 phase B study, and a discussion of the results. In this work a mechanical and thermal model is created, view factors and loadcases are defined, and material parameters are established. In general, the results show that the NSAT-1 could be realized from a thermal-mechanical point of view, using the suggested design. However the requirement of 1.0 E-3 deg maximum variation of the angle between the optical axis of the star tracker and the antenna boresight are too strict, and must be negotiated in the total error budget.

9) DATE	AUTHORIZED BY This page only	POSITION
21. February 2003	Bjørn Bergersen	Assistant Director

ISBN 82-464-0711-2

UNCLASSIFIED

SECURITY CLASSIFICATION OF THIS PAGE (when data entered)

CONTENTS

THERMAL AND MECHANICAL ANALYSES FOR THE NSAT-1 PHASE B STUDY

1 INTRODUCTION

From introduction of "New micro-satellite based concept for monitoring of maritime traffic by navigation radar detection, in Proceedings of the 8th International symposium on Remote Sensing"[1]: *Maritime issues play a vital role in Norway. Fisheries and shipping have for a long time been key economic factors. Today, export of oil and gas also is of primary importance. The Schengen agreement requires control of the outer national borders, this includes control with the naval traffic entering and leaving the economic zone. Norway has national jurisdiction in the 200-miles economic zone, the fisheries protection zone around Spitzbergen, and the fisheries zone around Jan Mayen. Certainly, a control regime must be in place.*

Radar satellite images have proved useful in maritime surveillance, but they are hampered by limited area coverage and long revisit time. The rational for the NSAT-1 mission is to develop a micro satellite with an advanced sensor for large-area detection and geolocation of vessels. According to the International Convention for Safety of Life at Sea (SOLAS), all ships larger than 45 m are required to use an X-band navigation radar. The Norwegian Defence Research Establishment (FFI) and industry partners are looking into a possible development of a micro satellite system with an X-band vessel-detector antenna to geolocation vessels in a 1000 km wide ground track.

The NSAT-1 concept is shown in figure 1.1.

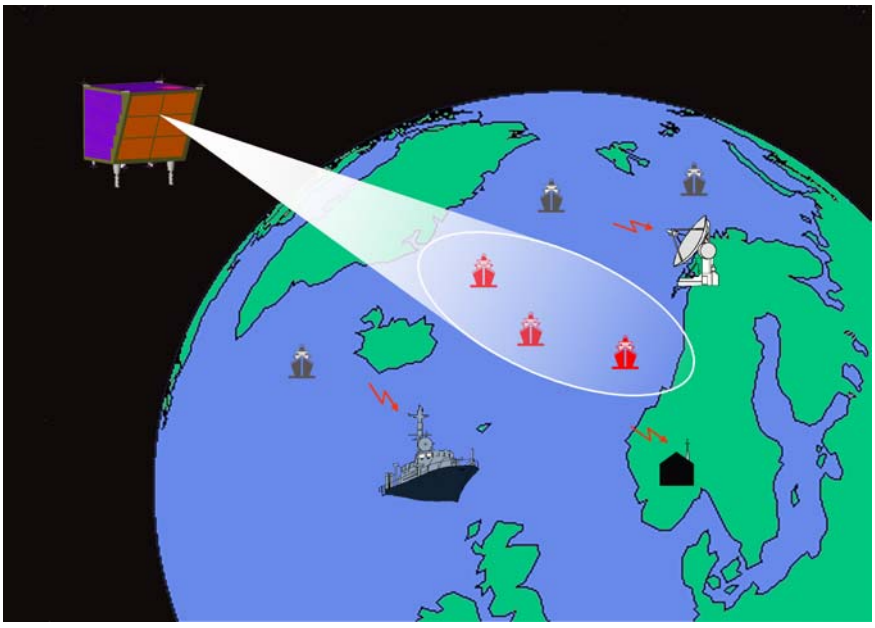

Figure 1.1 The concept of the Norwegian surveillance micro satellite, NSAT-1.

To achieve high geolocation accuracy, the pointing direction of the vessel-detector antenna has to be known with an extreme accuracy. A star tracker mounted to the backside of the antenna panel is the sensor used to determine the exact pointing direction of the antenna. Precise knowledge of the orientation of the star tracker relative to the antenna is essential. A critical component in this respect is a bracket connecting the star tracker to the antenna panel with a fixed angle between the optical axis of the star tracker and the antenna boresight[1]. This angle will vary due to thermal deformations in the star tracker housing, in the components (mainly the bracket described above) connecting the star tracker to the backside of the antenna panel, and in the antenna panel itself. This angular variation must be kept within strict requirements.

Several preliminary FE-analyses, both thermal and mechanical, have been done in the phase-A study [2].

In this phase B study, it is focused on the star tracker/antenna assembly and the mechanical requirements with respect to; the mounting bracket stability, the antenna flatness and the star tracker operation temperatures [3], [18]:

Mechanical:

- Total variation of angle between the optical axis of the star tracker and the antenna boresight (around the satellite y-axis, ref. Fig.3.1): 1.0 E-3 deg[2].
- Star tracker assembly first fundamental frequency: Above 100Hz.
- Star tracker assembly quasi-static loads (all combinations must be considered):

Direction	**g-level**
Parallel to mounting-plane	50
Perpendicular to mounting-plane	50

Table 1.1 Star tracker assembly quasi-static loads

- Antenna panel out-of-plane maximum deformation between phase centres: $\Delta = 10\mu m$.
- Antenna panel in-plane maximum deformation between phase centres: $\Delta = \pm 1500\mu m$.
- Antenna panel through plane maximum thickness change: $\Delta = 80\mu m$.

Thermal:

- Star tracker operating temperature: -35°C to +10°C.
- Star tracker mounting interface temperature variations during one orbit: $\Delta T = 4°C$.
- Star tracker temperature difference between any points on the mounting interface at any time: $\Delta T = 4°C$.

[1] The boresight is defined as the normal of the best fitted plane through the four phase centres at the antenna panel front side.

[2] Preliminary requirement, not stated in any specification. 0.00028deg is given in [3], but this was found to strict in later discussions [20]. The preliminary requirement of 1.0E-3 deg is kept.

These requirements are critical to the concept. In phase B more attention is also paid to the loadcases, describing detailed thermal loads both during power generation and observation.

The temperature distributions for solar panels and electronics are analyzed and evaluated on a general basis.

This report reveals the FE-modeling and analyses for the NSAT-1 phase B study, and a discussion of the results. A detailed background on material parameters and loadcases is found in the appendixes.

2 SATELLITE ORBIT AND ATTITUDE

The satellite is designed for a sun synchronous 18-06 low earth orbit, with an inclination of 98 deg. The altitude is set to 600 km, which corresponds to a cycle time of approximately 5800 seconds. For about 4900 seconds of an orbit the satellite is outside Norwegian waters, and will then be in power generation mode, with the solar panels pointing towards the sun, and the vessel-detector antenna pointing towards dark space. When reaching Norwegian waters, the satellite will switch to observation mode, pointing the vessel-detector antenna towards the sea.

The 18-06 orbit was chosen to ensure minimum temperature variations on the antenna panel during observation. In a 06-18 orbit, eclipse will occur over the North Pole around winter solstice. In this case the antenna panel will experience shifting solar loads when observing with the antenna panel pointing towards the sun, and hence problems with thermal expansions might occur. The different loadcases are described in detail in chapter 5.2.

3 SPACECRAFT DESIGN

The spacecraft body and internal deck are made of honeycomb panels, with a standard aluminium honeycomb core. Aluminium alloy is used for all skins, except for the antenna panel, which have carbon fibre composite skins. A high strength aluminium alloy is used for the launch adapter. All material data are given in Appendix C and D. The structure is self-supported and is assembled with adequate screws and inserts [4].

The solar panels experience large temperature variations, and are therefore mechanically and thermally loose-coupled to the satellite body. This allows them to expand freely, and it will ensure a more stable temperature in the rest of the spacecraft body and the internal electronics.

The dimensions of the cross-sectional area are 500 x 550 mm, and the height including the launch adapter is 709 mm. The total mass is 41.0 kg, without mounting and cables. This is all within the Ariane ASAP 5 requirements [5], which is used as a requirement baseline for the mechanical design. A CAD model of the entire satellite is shown in figure 3.1 and 3.2.

The star tracker is mounted to a titanium ring, which in turn is connected to the bracket with a carbon composite spacer. A radiator is attached to the star tracker for passive cooling, and a baffle shades for direct sunlight on the lenses. The baffle is thermally isolated from the titanium ring with a carbon composite ring. This assembly is shown in detail in figure 3.3.

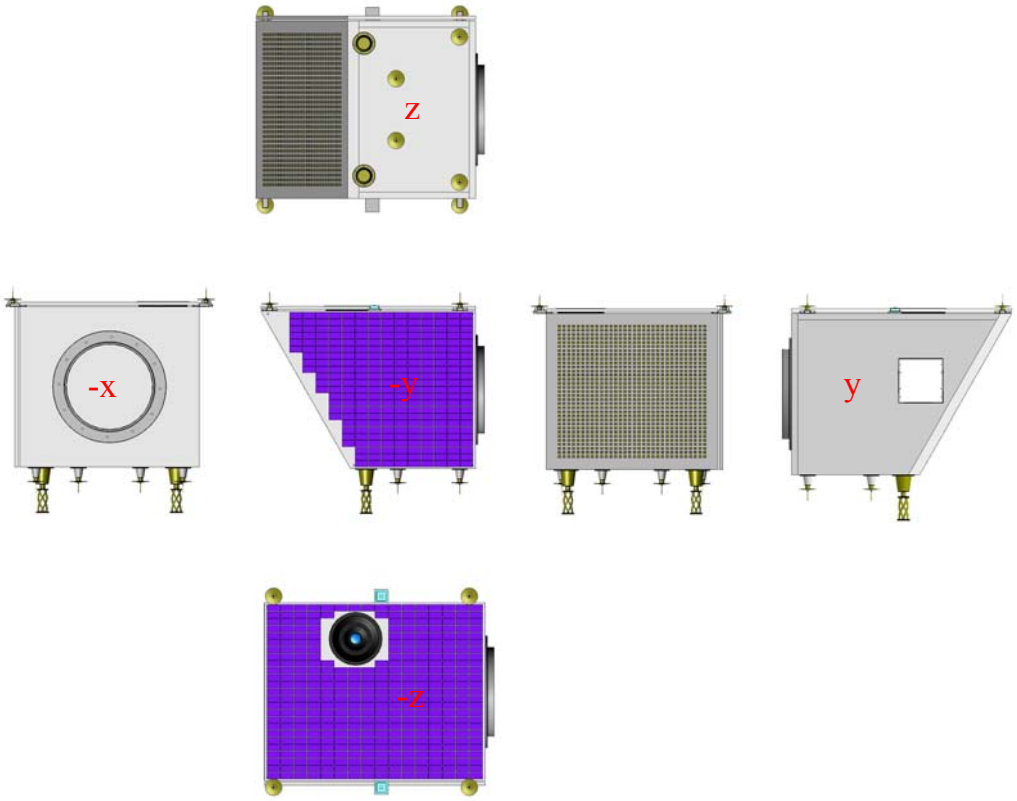

Figure 3.1 Satellite external views.

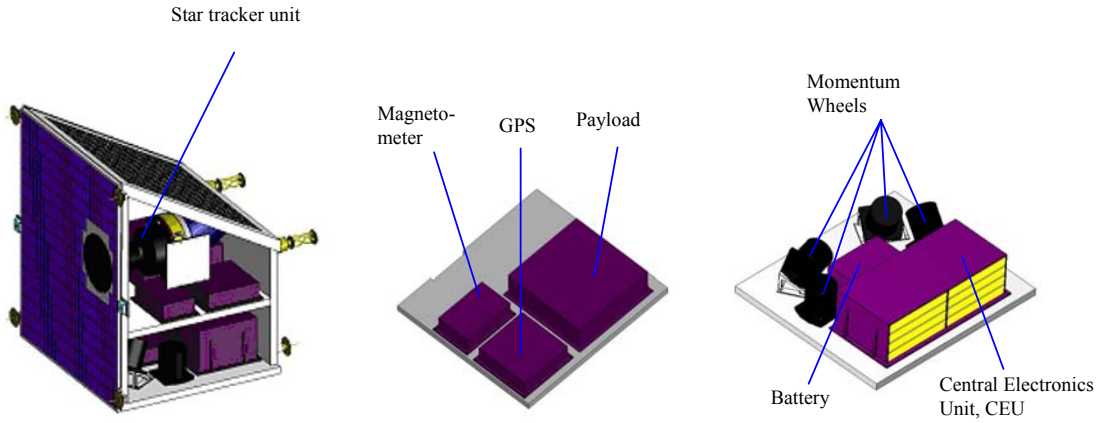

Figure 3.2 Satellite internal views.

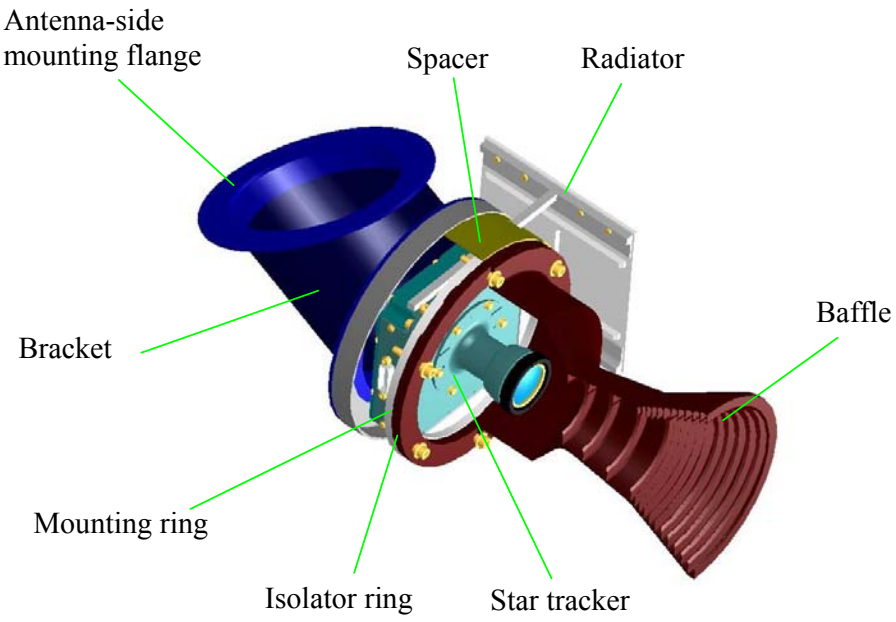

Figure 3.3 CAD model of star tracker assembly and bracket.
(Star tracker and baffle courtesy of Terma AS)

4 BRACKET DESIGN

4.1 Bracket layup and optimisation

As described in the introduction, the bracket connecting the star tracker assembly to the vessel-detector antenna is critical with respect to thermal-mechanical stability.

It seemed like a good idea to use carbon fibre composite in the bracket, and utilize the CTE-(Coefficient of Thermal Expansion) properties of carbon fibres. For a typical carbon fibre the CTE is positive across the fibre and negative along the fibre. A proper fibre layup will in theory give a zero CTE in a desired direction.

After some preliminary analyses on different geometries, a winded tube gave the best results. The tube is cut at each end with a certain angle (ref fig. 4.1), and with flanges glued on separately. By varying the layup angles this solution can be optimized for the desired stability.

The thermal stability requirement for the bracket is set with respect to angular variation between the two mounting flanges. This critical angle is shown in figure 4.1. The bracket is allowed to expand in any direction as long as it does not cause problems at the interfaces. The angular variation is a product of both radial and axial deformation.

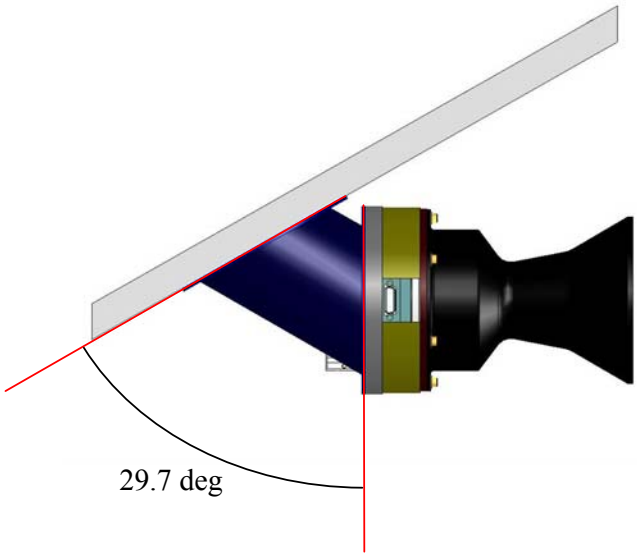

Figure 4.1 Critical angle between bracket mounting flanges.

A composite with 40% cyanate ester resin and 60% T-300 carbon fibre (with negative CTE along the fibre) were chosen. Given the CTE values, fibre fractions and Modulus of elasticity for both fibre and matrix, an equivalent CTE value for a single composite ply can be established [6].

Some simple hand calculations gave a brief idea on what a suitable layup would be. A hoop layer (90deg) in each end of the stack and some helical layers with approximately +/- 20 deg angle in the middle seemed reasonable. With this as a default layup, mechanical analyses on the bracket were run for different helical angles. The temperature load was uniform with a ΔT of 100 °C relative to the initial temperature. The angular variation between the flanges as function of layup angle for the helical layers is plotted in figure 4.2.

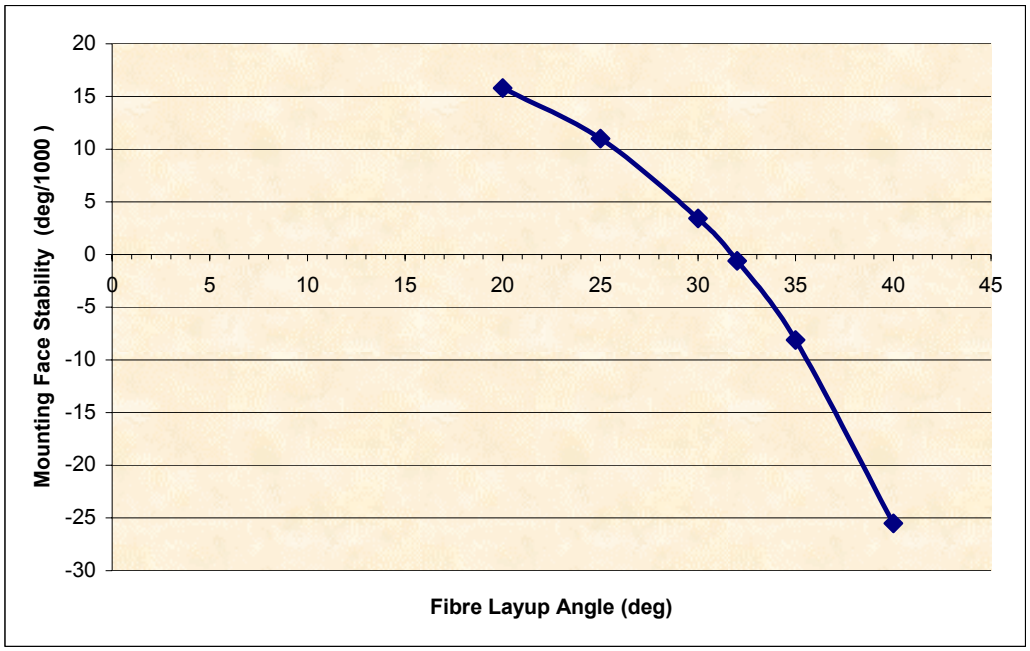

Figure 4.2 Angular variation between the flanges as function of helical layup angle for ΔT = 100 ℃.

A layup angle for the helical layers of +/-32 deg will give the best stability. The precision of the manufacturing process will typically be +/-1 deg. 32 deg is the nearest integer to the exact solution. The total layup is shown in table 4.1.

Ply number	Thickness (mm)	Layup angle
1	0.25	90 deg
2	0.28	+32 deg
3	0.28	-32 deg
4	0.28	+32 deg
5	0.28	-32 deg
6	0.25	90 deg

Table 4.1 Bracket carbon fibre composite layup.

The layup is used to create equivalent 2D conductivity values for the bracket for use in the thermal analyses (ref. App D).

4.2 Bracket and star tracker assembly mechanical verification

According to the mechanical requirements [3] the star tracker assembly shall have its first fundamental frequency above 100 Hz. Also it shall withstand a quasi-static design load of 50g parallel to antenna mounting-plane and 50g perpendicular to antenna mounting-plane. Also any combination of these loads must be considered.

The first fundamental frequency in the star tracker assembly appear in the radiator/heat pipe system at 135 Hz. The second fundamental frequency appears at 329 Hz, and is some coupled vibration between the baffle and the radiator. Both are shown in figure 4.3 and 4.4.

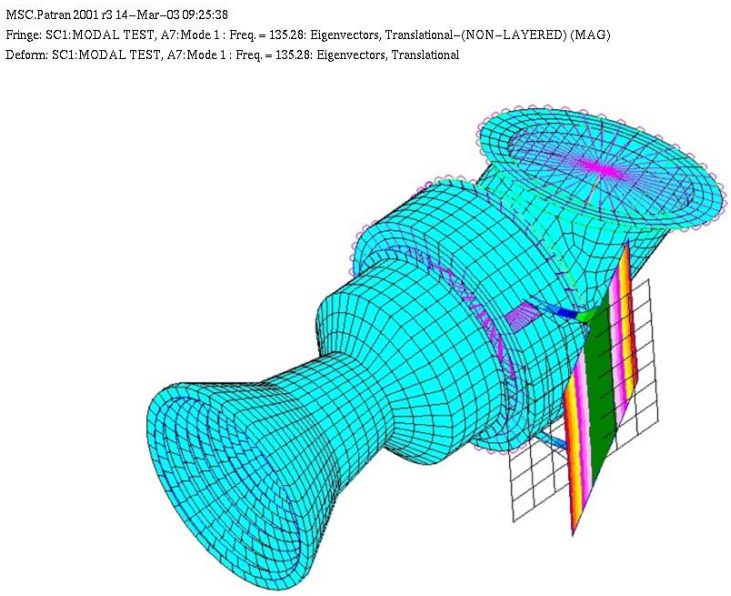

Figure 4.3 First fundamental frequency in the star tracker assembly at 135 Hz.

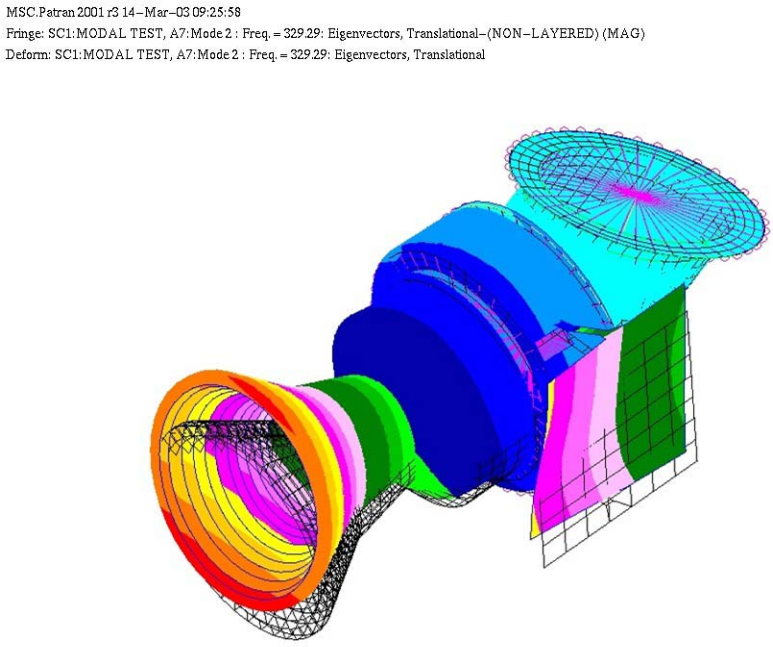

Figure 4.4 Second fundamental frequency in the star tracker assembly at 329 Hz.

Several load-combinations were analysed. “Worst-case” was found for two 50g loads in the antenna-side mounting-plane, appearing perpendicular to each other (axis -y and z in local coordinate system, fig. 4.5). The load perpendicular to the mounting-plane was zero in the “worst-case”.

The result of the quasi-static analysis was a maximum Von Mises stress of 69 MPa in the aluminium heat pipes connecting the radiator to the star tracker. This stress is not critical. The stresses in the bracket composite are compared to the “Maximum Stress Criterion” (ref. App. C), and margin of safety against fracture in the bracket is about 20.

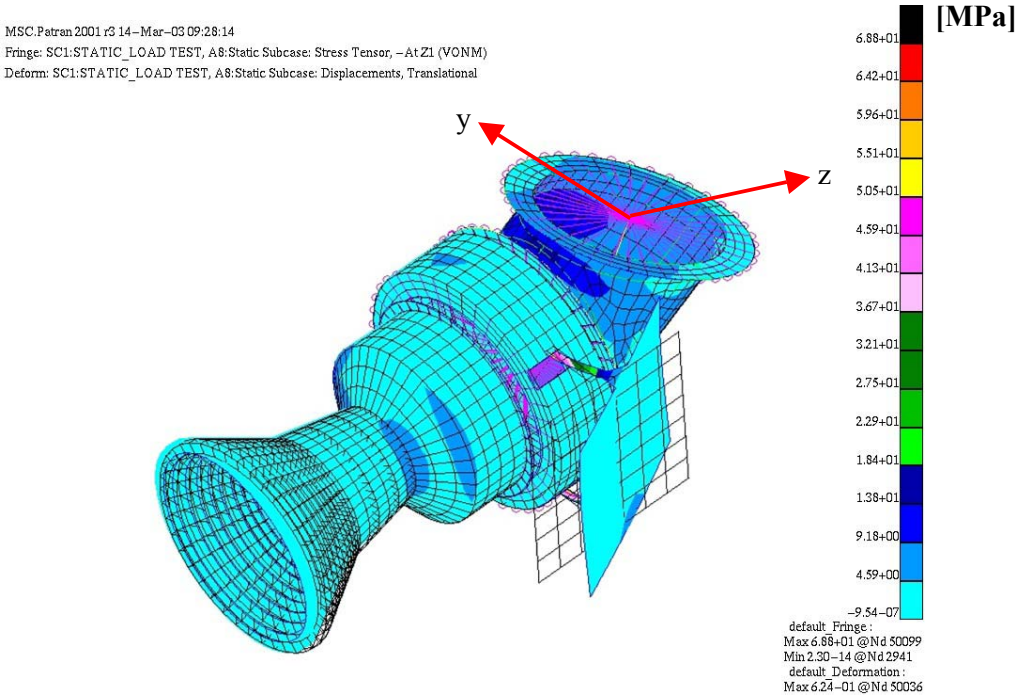

Figure 4.5 Quasi-static load acting on star tracker assembly.

The normal mode analyses and the quasi-static analyses show that the star tracker assembly fulfils the mechanical requirements [3]. Random vibration, shock and fatigue are not tested in this phase. The bracket itself is very solid. The weakest parts in the star tracker assembly are the heat pipes connecting the radiator to the star tracker. Note that none of the mechanical requirements in the ASAP5 [5], yielding for the entire satellite platform, are analysed for. Most of these analyses were carried out for the entire platform in the phase-A study. The requirements set for the star tracker assembly alone are stricter than the ASAP5 requirements, and new analyses on the complete platform are not considered necessary. All mechanical data are found in Appendix D.

5 THERMAL DESIGN AND ANALYSES

5.1 Thermal model description

The spacecraft honeycomb structure and solar panels are modelled with shell-elements (QUAD4). The launch adapter is neglected. For electronic boxes, only the component bottom plates are modelled, using shell elements. The density is adjusted so that the masses of the bottom plates equal the actual component masses. Hence the amount of heat stored in the components is correctly represented. The complete FE-model is shown in figure 5.1.

The star tracker assembly consists of: carbon fibre composite bracket, star tracker, aluminium radiator, carbon fibre composite spacer, titanium mounting ring, carbon fibre composite isolating ring and aluminium baffle. All these components are made of shell elements, except the star tracker, which are represented with 3 nodes only, and the isolating ring, which is modelled with 1D conductor elements (CELAS1). The star tracker assembly is connected to the backside of the antenna panel with the critical carbon fibre composite bracket. The bracket temperatures will depend on the antenna temperature in one end, and the baffle and star tracker temperatures in the opposite end. It is therefore desirable to keep the conductance at the bracket mounting flanges small. From the literature [7] and experiences from Terma AS [19], some realistic and conservative values are found (Ref. App. D).

The complete star tracker assembly can be seen in figure 5.1. Model details of the star tracker, radiator and mounting ring are shown in figure 5.2

The antenna panel is built up from inside to outside in the following way: structural panel with carbon fibre composite skins and aluminium honeycomb core, cyanate ester glue, Kevlar layer, cyanate ester glue and copper patches. The skins, the Kevlar layer and the patches are all made of shell elements. 1D conductor elements are used for the glue. The antenna panel honeycomb core is represented with solid elements (HEX8), because an accurate representation of heat transfer between the antenna front side and the sensitive bracket mounted on its backside is necessary. Details of the antenna FE-model can be seen in figure 5.3.

All panels and components are assembled with screws, modelled as 1D conductor elements. The distance between the screws is approximately 60 mm. All heat transfer between different components and panels in the model is due to conduction through these elements. Any interface fillers are corrected for in the conductance of the screws. Internal radiation is neglected since the temperature differences inside the satellite are relatively small.

The complete structure is represented by 24906 nodes and 34735 elements. All modelling and analyses are done with MSC.Patran and MSC.Nastran. Details on the thermal data used in the model can be found in appendix D.

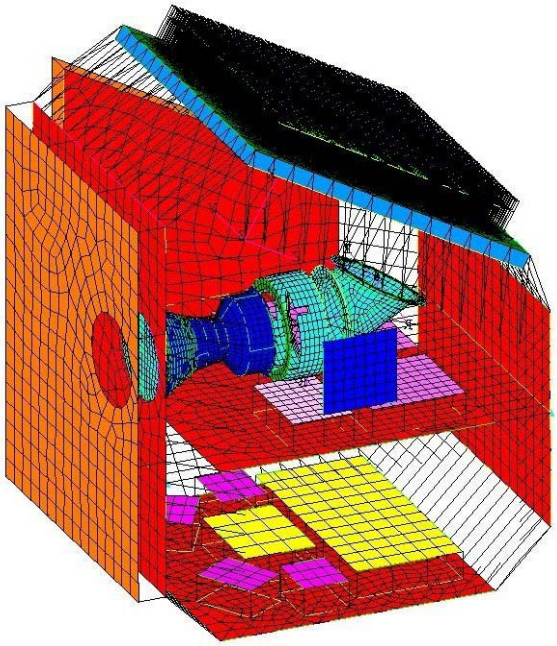

Figure 5.1 Complete finite element model (side panel hidden for internal view).

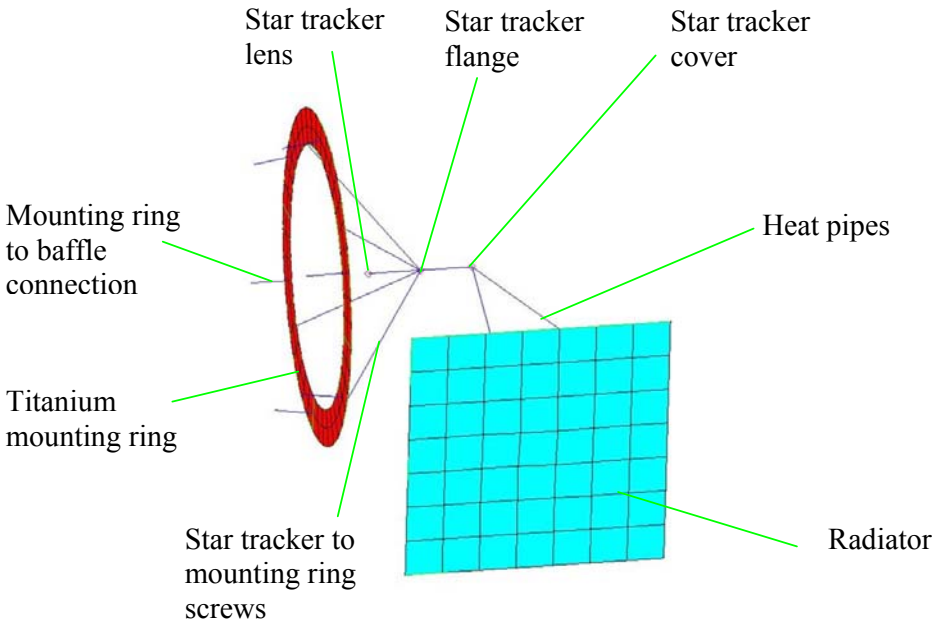

Figure 5.2 FE-model of star tracker, radiator and titanium mounting ring.

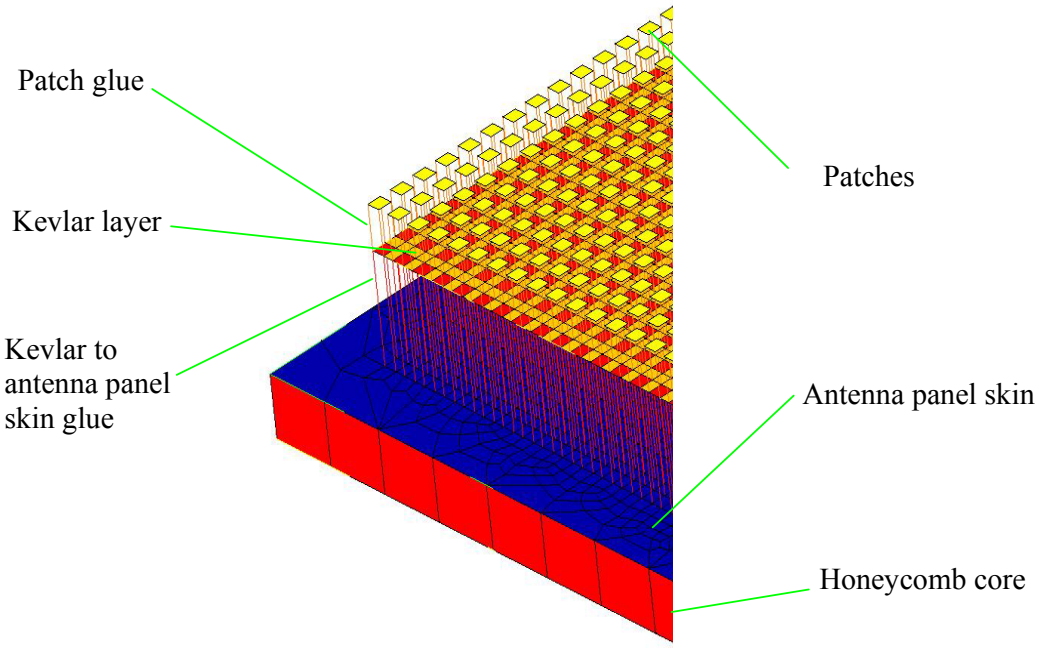

Figure 5.3 FE-model of antenna panel.

5.2 Thermal loads and loadcases

The temperature of any parts of the satellite structure will change remarkably when going from sun to shadow, and this can be a challenge with respect to thermal expansions and operation temperatures for sensitive equipment. The heat transfer mechanisms present in space are conduction and radiation.

The major heat input is the solar flux. Earth- IR and sunlight reflected by the earth (Albedo) will also have a significant contribution in low orbits like this. The electronics also dissipate some heat. In the energy budget this heat is a conversion of the electrical power generated by the solar panels, and it has to be subtracted from the incoming solar flux, not to be applied twice. The output is radiation to dark space. The amount of absorbed and emitted heat is regulated by the surface absorptivity and emissivity, which are dependent on the surface coating.

The temperature distribution within the satellite will depend on internal radiation, and how heat is conducted throughout the structure. The temperature differences between the electronic boxes will in general be small. The sensitive star tracker assembly will be wrapped in MLI (Multi Layer Insulation), and this can also be done to the inside of the structural panels. Therefore internal radiation is neglected. The responses to the different transient loads depend on the heat capacity of the components.

The satellite orbit can be divided into two phases. For 4900 seconds of an orbit the satellite will be in power generation modus with an incident solar angle of 50 deg on the large solar panel (-z, ref. Fig. 3.1) and 40 deg on the small solar panel (90 deg being normal to the panel). For the remaining 900 seconds the satellite is in observation modus.

During power generation the satellite can operate in two different attitude modes. In “Mode1” the satellite attitude is fixed relative to an earth fixed coordinate system. In “Mode2” the satellite attitude is rotating relative to an earth fixed coordinate system, always pointing its bottom plate (-x, ref. Fig. 3.1) towards the earth. This is illustrated in figure 5.4.

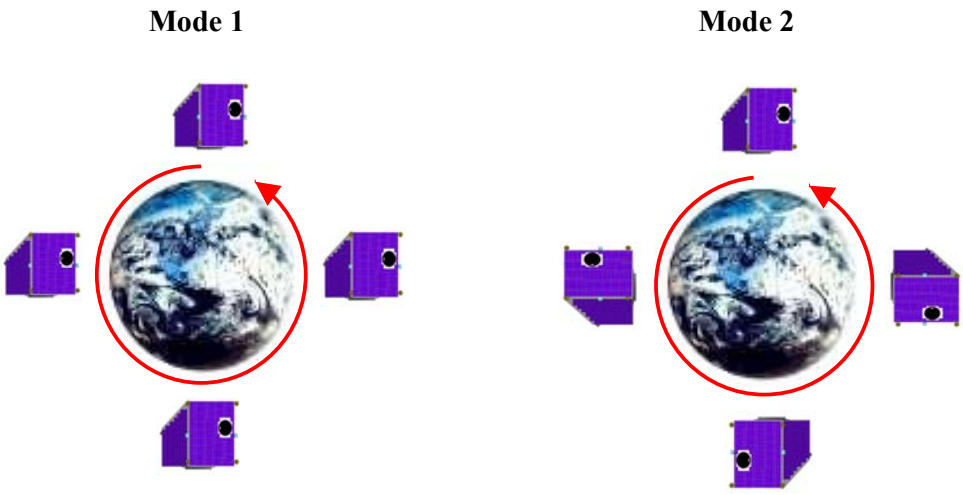

Figure 5.4 Power generation attitude mode1 and 2.

For the observation period three different observation modes are possible:

- Side-looking observation with antenna panel pointing towards sun.
- Side-looking observation with antenna panel pointing away from sun.
- Target-pointing observation with antenna panel fixing on a target.

These three observation modes combined with two different power generation modes, gives a total of six loadcases.

Due to the 23.4 deg tilt of the earth’s pole axis with respect to the normal of the ecliptic plane, the projection of the orbit seen from the sun will vary throughout the year. This will cause some load variations, and it is necessary to find an annual “worst-case”

When observing side-looking with the antenna panel pointing towards the sun, the “hot-case” with respect to the antenna and the star tracker assembly occur at winter solstice, with use of end of life (EOL) absorbtivity values. In this case the antenna panel is switching from facing dark space in power generation mode, to being directly exposed to the sun under observation, with an incident angle of 75 deg (90 deg being normal to the panel). The temperature variation in the bracket due to conduction through the antenna/bracket interface is then at its maximum.

Since the antenna and the star tracker assembly are the most critical components with respect to large temperature transients, winter solstice is used as the annual “worst-case”

The “cold-case” with respect to the antenna and the star tracker assembly will obviously be for a side looking observation with the antenna panel pointing away from sun, with the use of beginning of life (BOL) absorbtivity values.

For the star tracker operating temperature, the target-pointing observation mode is critical since the radiator in this case for a short period will be exposed to sunlight.

With respect to the two different power-generation modes, there are significant differences in albedo and IR-loads between the two modes. “Mode1” gives continuously varying view factors to earth for all sides during power generation, and hence large orbital variations of albedo and IR. “Mode2” gives nearly constant view factors to earth, and will not expose the antenna panel to albedo or IR during power generation.

It is necessary to analyse all six loadcases. Different loadcases are critical for different parts. All loadcases are given in Appendix A.

The value of solar flux is assumed constant. The earth IR and Albedo are both functions of time of the year and of latitude [7]. For the earth IR the geographic variations are small, and an average value for December (winter solstice) is used (ref. Table B.1). The albedo for the given orbit parameters at winter solstice, will only occur at the southern hemisphere. A December albedo curve as function of latitude for the given orbit is created (ref. Table. B.2).

The tricky part is to generate view-factor curves for power generation “mode 1”, for each side of the satellite. The view-factors change continuously with the satellite attitude during an orbit. The albedo and IR loads are multiplied with the earth view-factor curves. The same curves are used for the radiation loads, to tell the fraction of earth/space in the field of view. The view-factor curves to earth are given in figure 5.5. More details on how the view-factor curves are created can be found in Appendix B.

The loadcase is used in an MSC.Nastran thermal transient analysis (sol.159) and run for 15 orbits to ensure convergence.

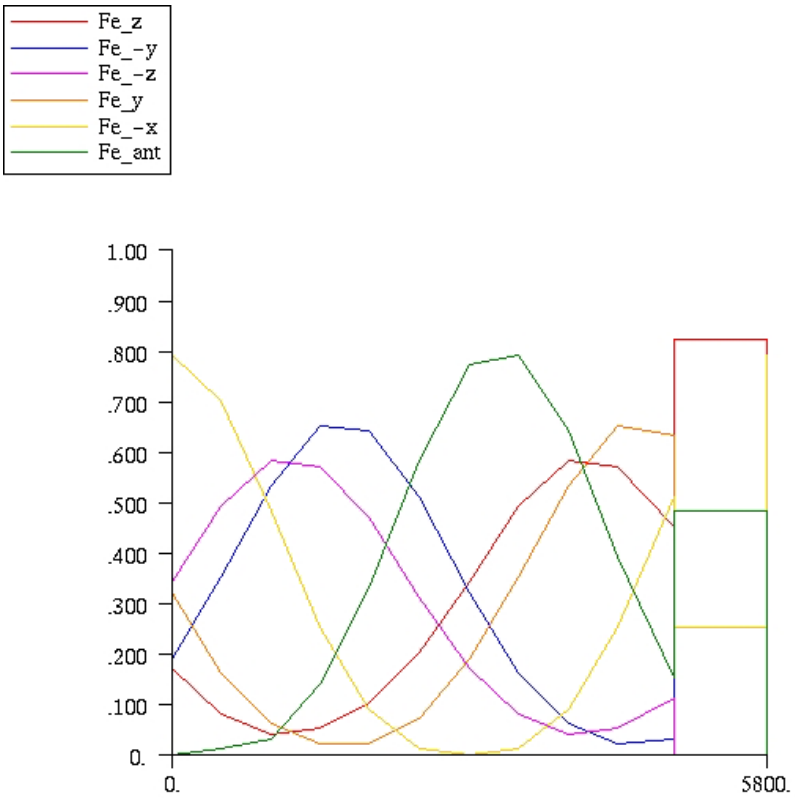

Figure 5.5 View factors to earth for each side of satellite for power generation "mode 1".

5.3 Thermal results and discussion

All six loadcases described in chapter 5.2 are analysed for. The thermal results for different parts of the satellite are given in the following sub-chapters.

5.3.1 Antenna thermal results

For the antenna panel the maximum and minimum operating temperatures during observation must be found for use in the thermal-mechanical analyses. Also the absolute maximum and minimum temperatures during an entire orbit, and the temperature variation across the panel during observation, must be identified.

5.3.1.1 Antenna thermal results for power generation "mode 1"

Antenna temperatures are given for the patches and for the back of the antenna panel. For the patches temperature curves for one orbit is plotted for one patch in the middle (element 57695, magenta curve), and for the four corner patches. This is shown in figure 5.6 for "hot-case", and figure 5.8 for "cold-case". For the back of the antenna panel, the same temperature curves are given for positions corresponding to the patch positions (the centre position on the back side is element 43744, magenta curve). This is shown in figure 5.7 for "hot-case" and 5.9 for "cold-case".

"Hot-case":

The side-looking loadcase when observing towards the sun, and with use of EOL absorptivity values, will give the antenna maximum operating temperature.

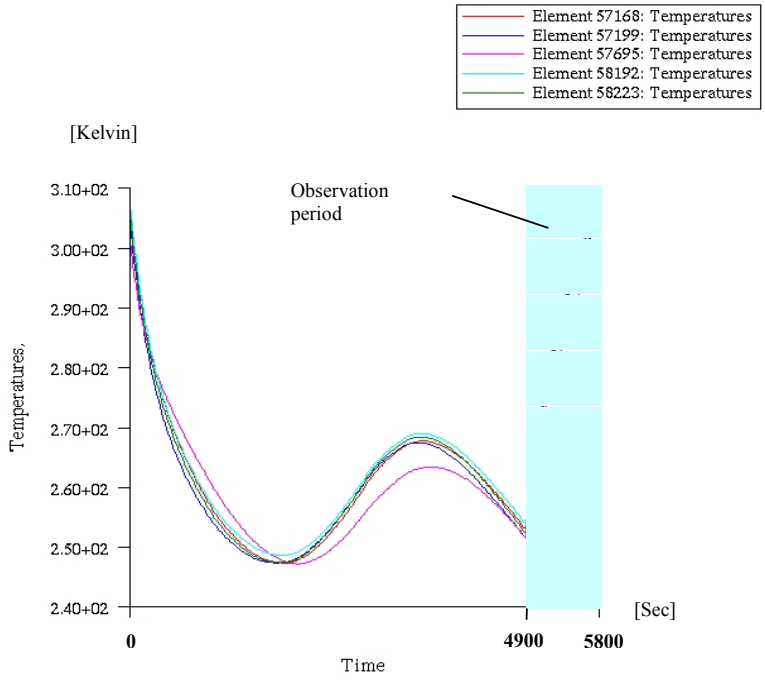

Figure 5.6 "hot-case" temperatures in centre and corner patches on antenna panel for power generation mode1.

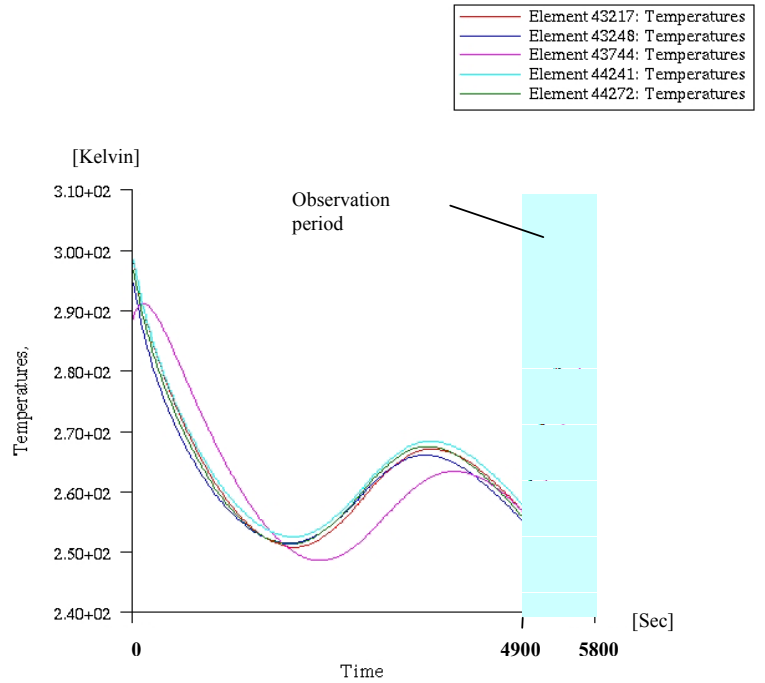

Figure 5.7 "hot-case" temperatures on the back of the antenna panel for power generation mode1, corresponding to patch positions in figure 5.6.

"Cold-case":

The side-looking loadcase when looking away from sun, and with use of BOL absorptivity values, will give the minimum operating temperature.

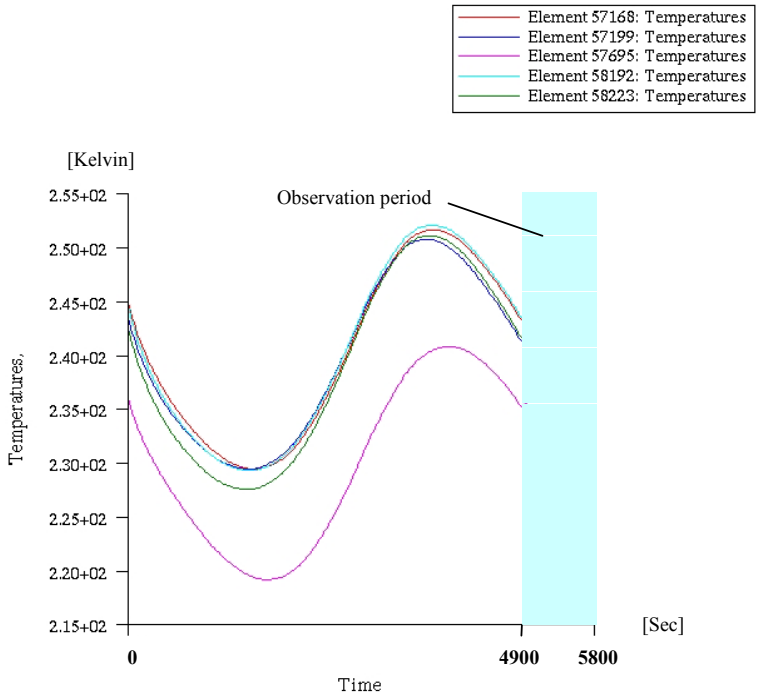

Figure 5.8" Cold-case" temperatures in centre and corner patches on antenna panel for power generation mode1.

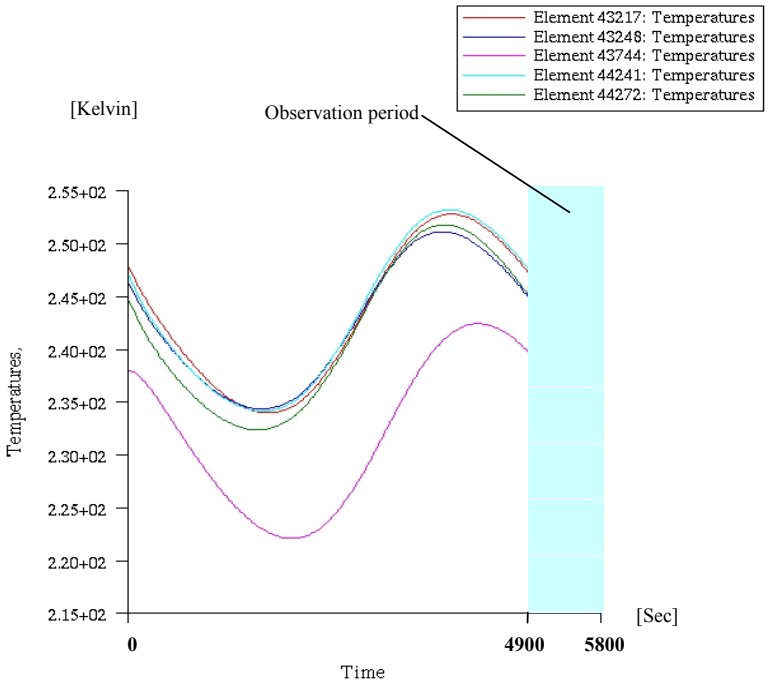

Figure 5.9 "Cold-case" temperatures on the back of the antenna panel for power generation mode1, corresponding to patch positions in figure 5.8.

5.3.1.2 Antenna thermal results for power generation “mode 2”

Antenna temperatures are given for the patches and for the back of the antenna panel. For the patches temperature curves for one orbit is plotted for one patch in the middle (element 57695, magenta curve), and for the four corner patches. This is shown in figure 5.10 for “hot-case”, and figure 5.12 for “cold-case”. For the back of the antenna panel, the same temperature curves are given for positions corresponding to the patch positions (the centre position on the back side is element 43744, magenta curve). This is shown in figure 5.11 for “hot-case”, and figure 5.13 for “cold-case”.

“Hot-case”:
The side-looking loadcase when observing towards the sun, and with use of EOL absorptivity values, will give the antenna maximum operating temperature.

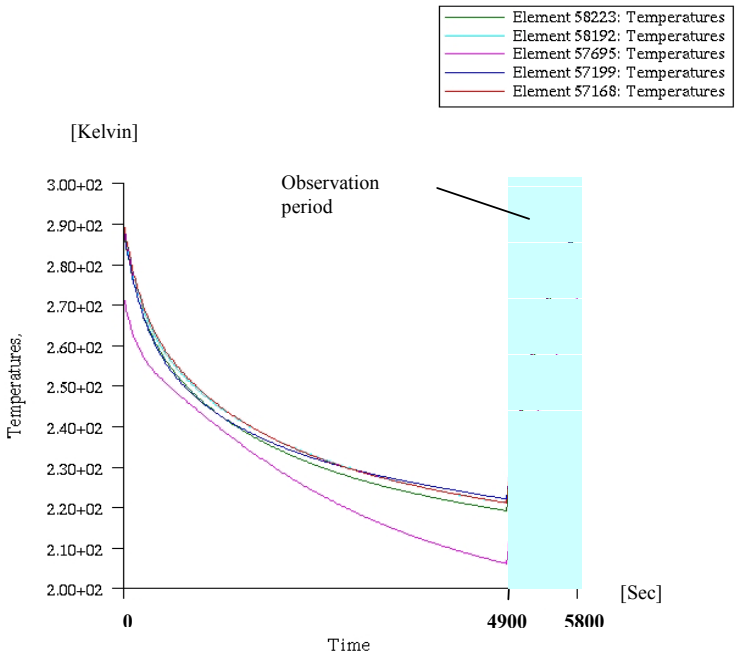

Figure 5.10 “hot-case” temperatures in centre and corner patches on antenna panel for power generation mode2.

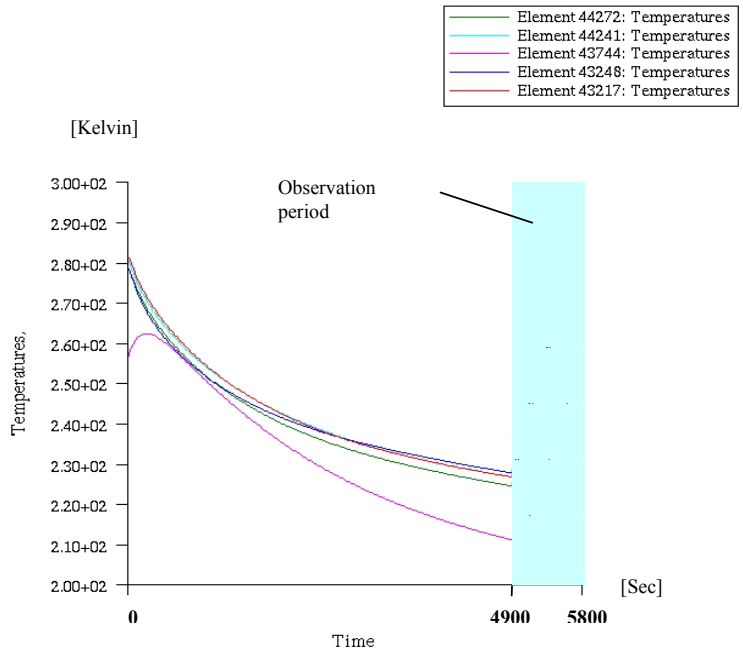

Figure 5.11 "hot-case" temperatures on the back of the antenna panel for power generation mode2, corresponding to patch positions in figure 5.10.

"Cold-case":

The side-looking loadcase when looking away from sun, and with use of BOL absorptivity values, will give the minimum operating temperature.

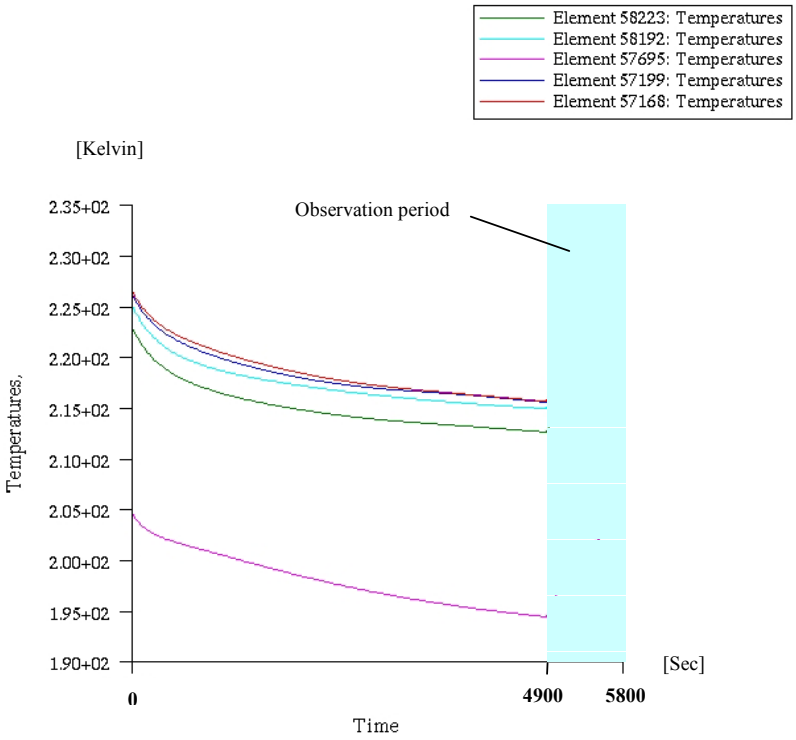

Figure 5.12 "Cold-case" temperatures in centre and corner patches on antenna panel for power generation mode2.

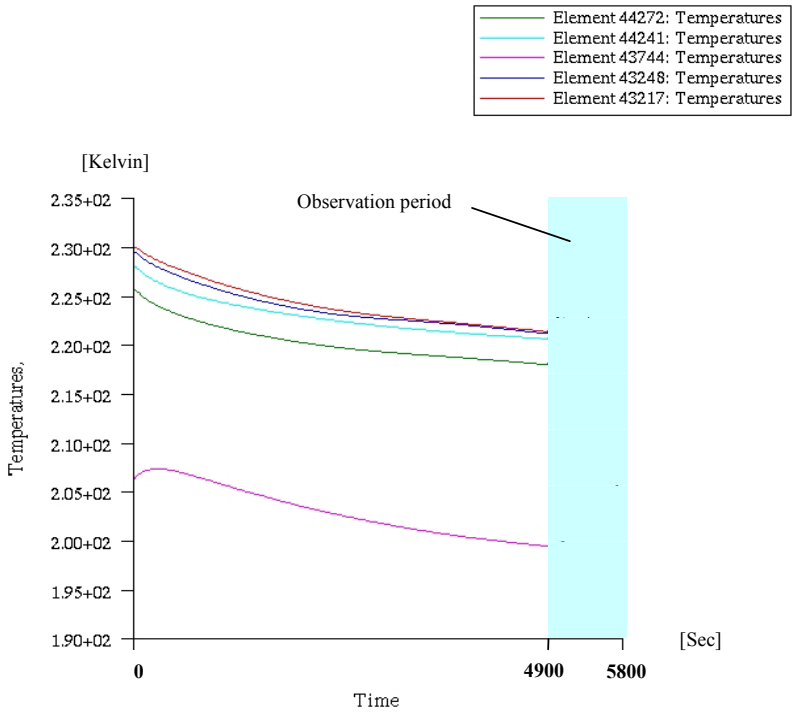

Figure 5.13 "Cold-case" temperatures on the back of the antenna panel for power generation mode2, corresponding to patch positions in figure 5.12.

5.3.1.3 Antenna results summary

	Power generation "mode 1"	**Power generation "mode 2"**
Absolute maximum temperature	+34°C at a corner patch Observation towards sun	+17°C at a corner patch Observation towards sun
Absolute minimum temperature	-54°C at the centre patches Observation away from sun	-78°C at the centre patches Observation away from sun
Observation maximum temperature	+34°C at a corner patch Observation towards sun	+17°C at a corner patch Observation towards sun
Observation minimum temperature	-37°C at the centre patches Observation away from sun	-78°C at the centre patches Observation away from sun
Maximum temperature variation during observation at a given location on the surface.	ΔT = 53°C at a corner patch Observation towards sun	ΔT = 68°C at a corner patch Observation towards sun
Maximum temperature difference between two locations on the surface at a given time during observation	ΔT = 9°C Observation away from sun	ΔT = 22°C Observation away from sun
Max temperature difference through panel thickness at given location on the surface at a given time during observation	ΔT = 14°C Observation towards sun	ΔT = 15°C Observation towards sun

Table 5.1 Antenna results summary

5.3.2 Bracket thermal results

For the bracket it is only of interest to find the largest temperature variations during observation. For side-looking observation towards the sun, the antenna panel is switching from seeing dark space in both power generation modes, to see almost directly into the sun. The temperature variations in the bracket due to conduction through the antenna/bracket interface will then be at its maximum.

5.3.2.1 Bracket thermal results for power generation “mode 1”

Maximum bracket temperature variations during an orbit for side-looking observation towards the sun for power generation “mode 1” are given in figure 5.14.

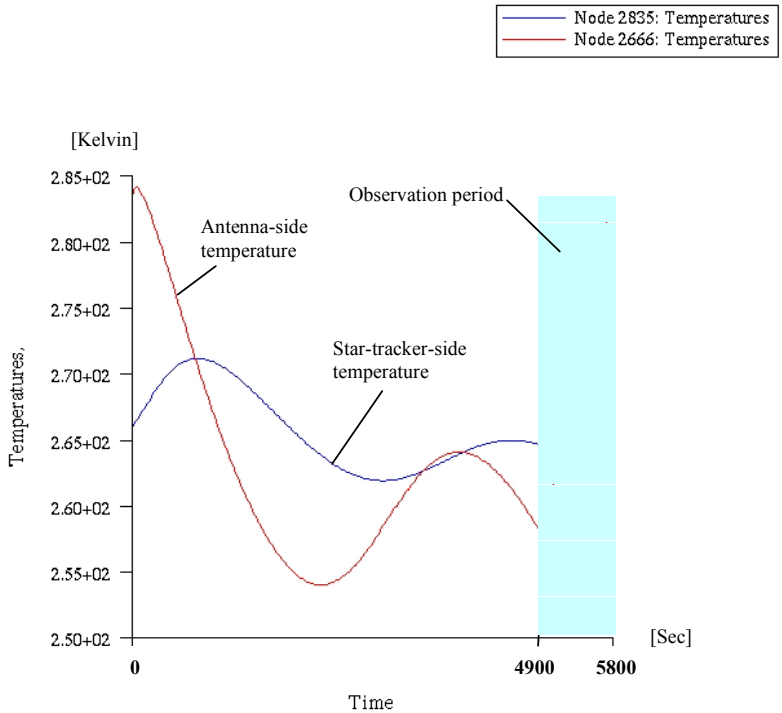

Figure 5.14 Bracket temperatures for side looking observation towards the sun, power generation “mode 1”.

5.3.2.2 Bracket thermal results for power generation “mode 2”

Maximum bracket temperature variations during an orbit for side-looking observation towards the sun, power generation “mode 2”, are given in figure 5.15.

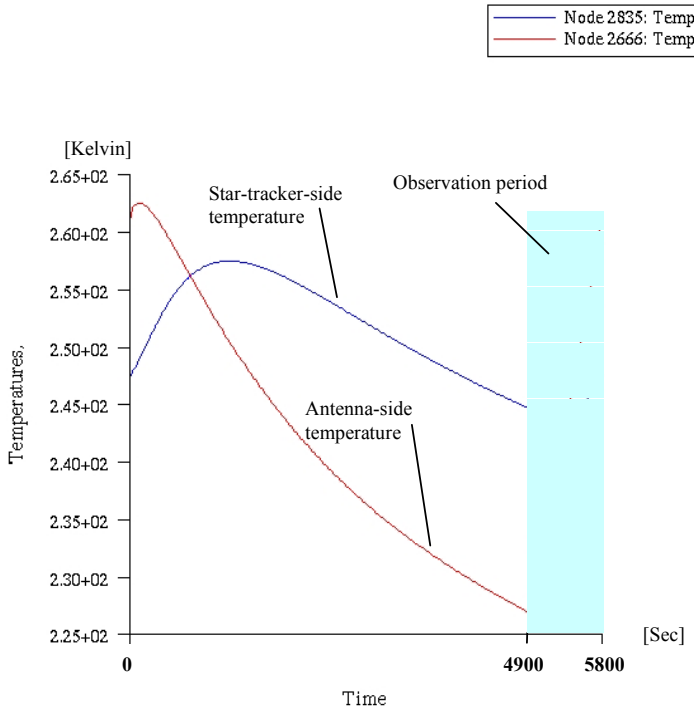

Figure 5.15 Bracket temperatures for side looking observation towards the sun, power generation “mode 2”.

5.3.2.3 Bracket results summary

	Power generation “mode 1”	**Power generation “mode 2”**
Observation maximum temperature at star-tracker-side	-6°C Observation towards sun	-25°C Observation towards sun
Observation minimum temperature at star-tracker-side	-7°C Observation towards sun	-29°C Observation towards sun
Observation maximum temperature at antenna-side	+11°C Observation towards sun	-11°C Observation towards sun
Observation minimum temperature at antenna-side	-15°C Observation towards sun	-46°C Observation towards sun

Table 5.2 Bracket results summary

5.3.3 Star tracker results

The star tracker temperature is at its maximum for target pointing observation because the radiator will be exposed to the sun for a short time. For this “hot-case”, EOL absorptivity values are used for the radiator and the antenna panel. The star tracker temperature is at its minimum for side-looking observation away from the sun, because the amount of heat

conducted from the antenna panel through the bracket is at its minimum for this observation mode. In this case, BOL absorptivity values are used for the radiator and the antenna panel.

Power generation “mode 1” demands a larger radiator because the radiator during parts of the orbit will be exposed to larger IR and albedo loads than in “mode 2”. The “hot”- and “cold-cases” for both power generation modes are shown in figures 5.16-5.19.

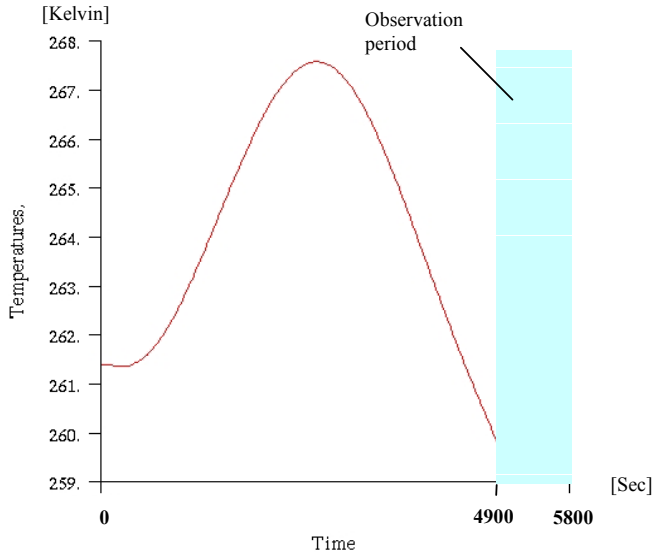

Figure 5.16 Star tracker “hot-case” temperatures for target-pointing observation, power generation “mode 1”.

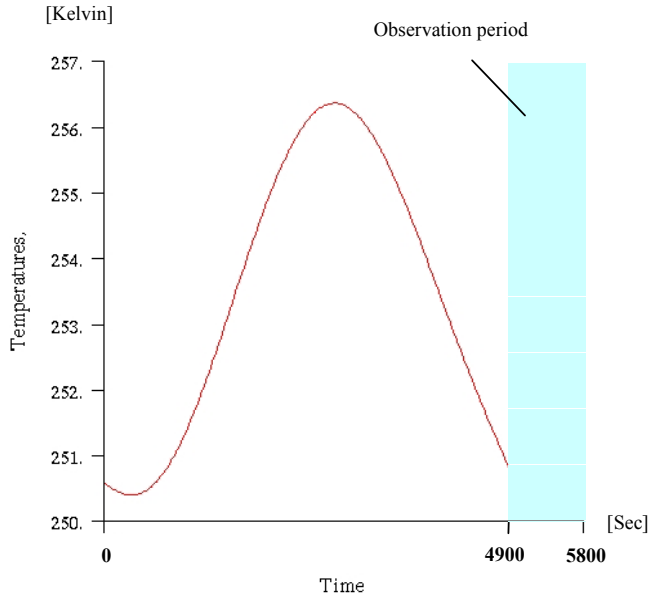

Figure 5.17 Star tracker “cold-case” temperatures for side-looking observation away from sun, power generation “mode 1”.

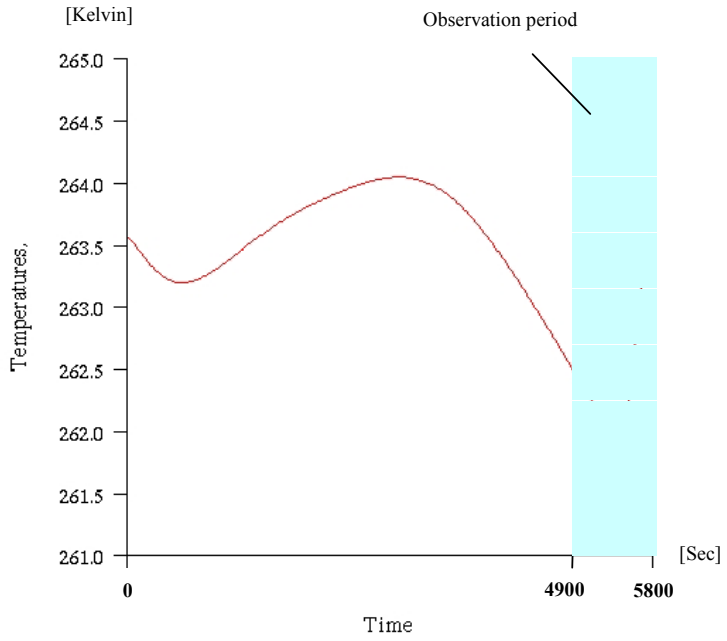

Figure 5.18 Star tracker "hot-case" temperatures for target-pointing observation, power generation "mode 2".

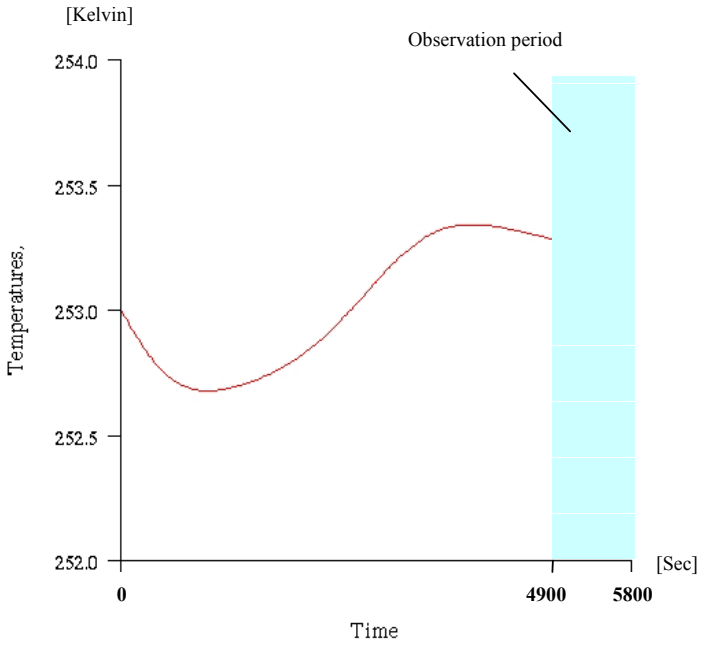

Figure 5.19 Star tracker "cold-case" temperatures for side-looking observation away from sun, power generation "mode 2".

5.3.3.1 Star tracker results summary

	Power generation "mode 1"	**Power generation "mode 2"**
Absolute maximum temperature	-5°C Target-pointing observation	-9°C Target-pointing observation
Absolute minimum temperature	-23°C Observation away from sun	-20°C Observation away from sun
Observation maximum temperature	-12°C Target-pointing observation	-9°C Target-pointing observation
Observation minimum temperature	-22°C Observation away from sun	-20°C Observation away from sun
Maximum temperature change during observation	ΔT = 2°C Target-pointing observation	ΔT = 2°C Target-pointing observation
Maximum temperature change during an orbit	ΔT = 8°C Target-pointing observation	ΔT = 2°C Target-pointing observation

Table 5.3 Star tracker results summary

5.3.4 Solar panels results

The results for the solar panels are independent of the observation mode. Figure 5.20 and 5.21 show temperatures for solar panels in power generation "mode 1" and "mode 2".

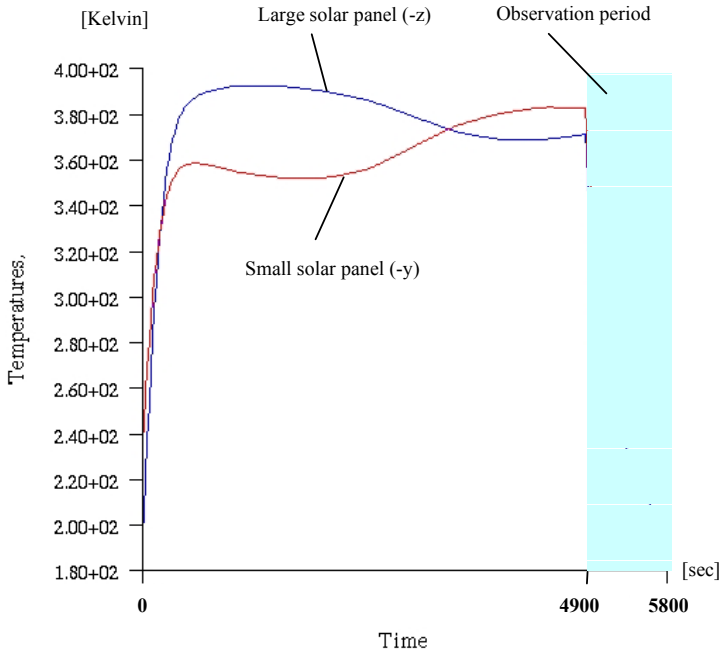

Figure 5.20 Solar panel temperatures for power generation "mode 1".

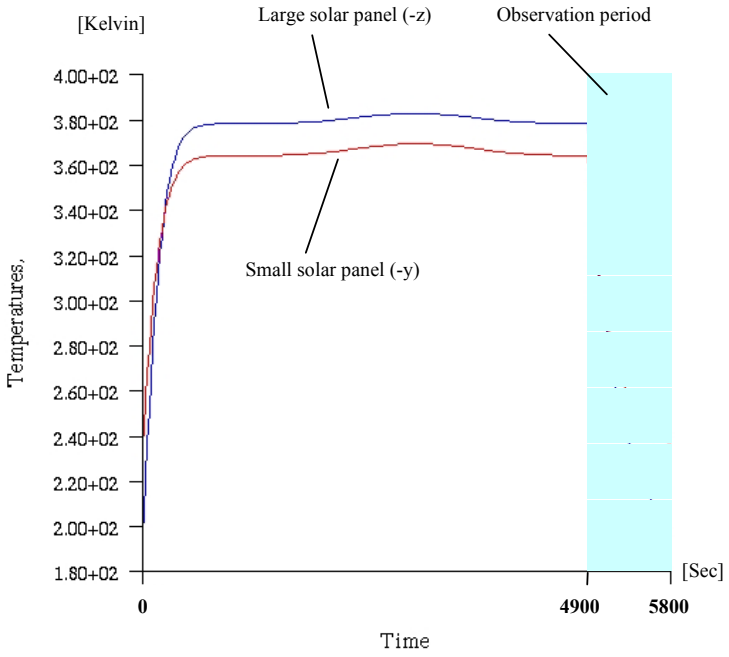

Figure 5.21 Solar panel temperatures for power generation "mode 2".

5.3.4.1 Solar panels results summary

	Power generation "mode 1"	**Power generation "mode 2"**
Maximum temperature during power generation, large solar panel	+119°C	+110°C
Minimum temperature during power generation, large solar panel	-78°C	-77°C
Maximum temperature during power generation, small solar panel	+109°C	+96°C
Minimum temperature during power generation, small solar panel	-36°C	-36°C

Table 5.4 Solar panels results summary

5.3.5 Electronics results

For the electronics, the "hot-case" occurs for side-looking observation away from the sun. At this time the bottom deck is pointing directly to the sun, and is therefore heated. The "cold-case" will be the opposite, when observing with antenna pointing towards the sun, and the bottom deck pointing mostly towards dark space. "Hot"- and "cold-case" temperatures are given for both power generation modes in figures 5.22-5.25. The element temperatures plotted for each curve represents the following:

- Element 1742: Payload
- Element 1821: GPS
- Element 1875: Magnetometer
- Element 4693: Battery
- Element 4740: CEU (Central Electronics Unit)
- Element 4789: Momentum wheels

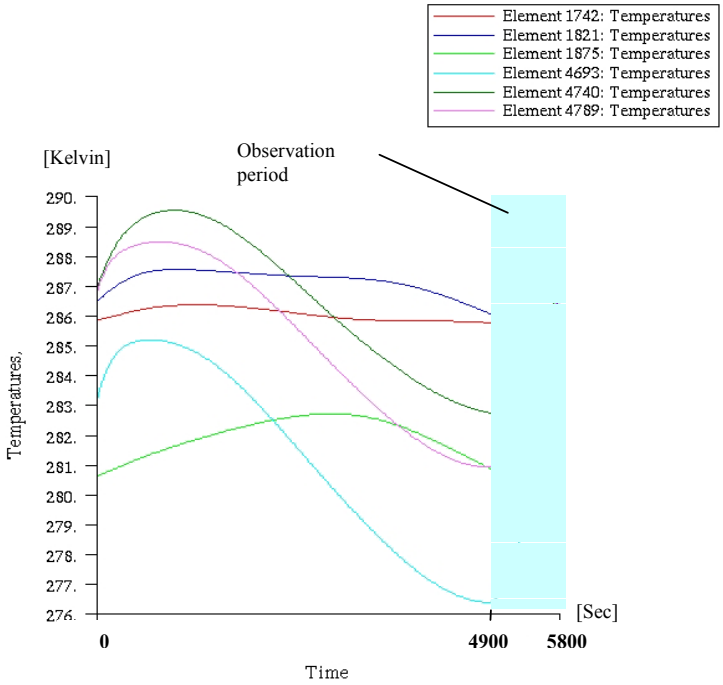

Figure 5.22 Electronics "hot-case" temperatures, power generation "mode 1".

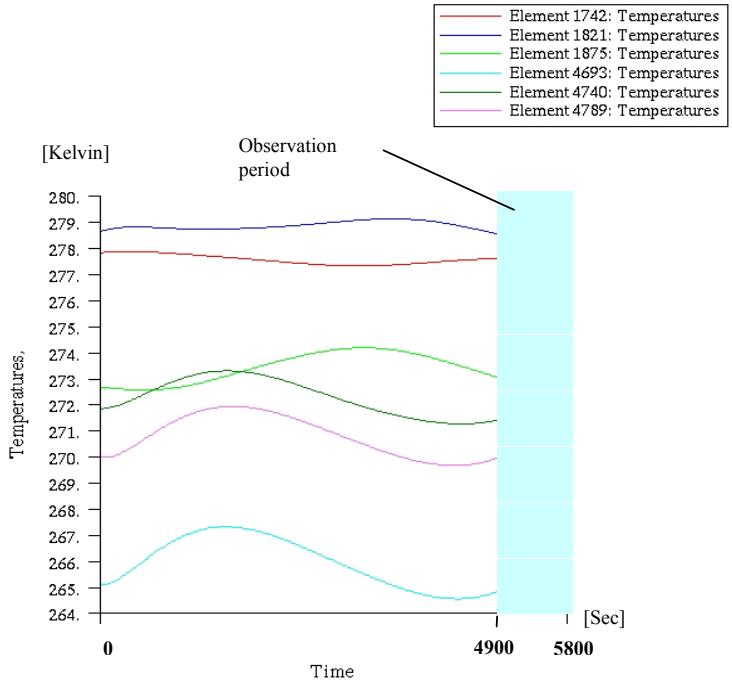

Figure 5.23 Electronics "cold-case" temperatures, power generation "mode 1".

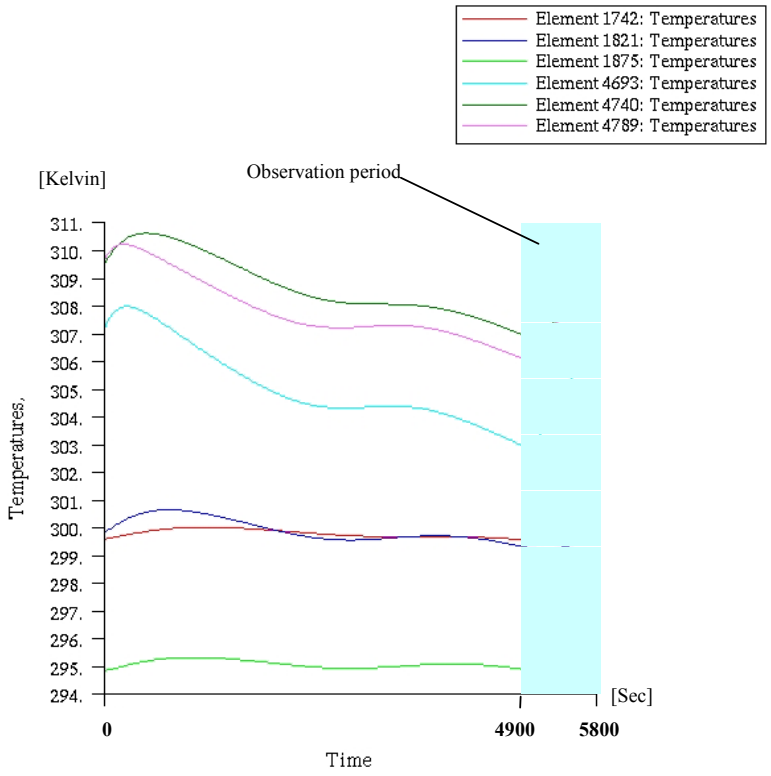

Figure 5.24 Electronics "hot-case" temperatures, power generation "mode 2".

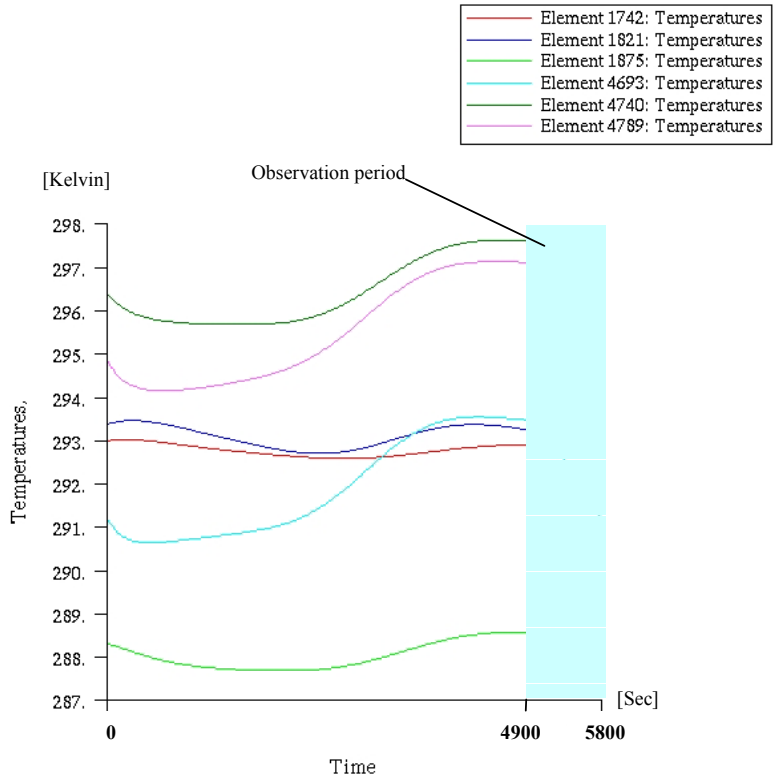

Figure 5.25 Electronics "cold-case" temperatures, power generation "mode 2".

5.3.5.1 Electronics results summary

	Power generation "mode 1"	**Power generation "mode 2"**
Payload maximum / minimum temperature, "hot-case"	+13 / +13°C Observation away from sun	+27 / +27°C Observation away from sun
Payload maximum / minimum temperature, "cold-case"	+5 / +4°C Observation towards sun	+20 / +20°C Observation towards sun
GPS maximum / minimum temperature, "hot-case"	+15 / +13°C Observation away from sun	+28 / +26°C Observation away from sun
GPS maximum / minimum temperature, "cold-case"	+6 / +5°C Observation towards sun	+21 / +20°C Observation towards sun
Magnetometer maximum / minimum temperature, "hot-case"	+10 / +8°C Observation away from sun	+23 / +22°C Observation away from sun
Magnetometer maximum / minimum temperature, "cold-case"	+1 / 0°C Observation towards sun	+15 / +16°C Observation towards sun
Battery maximum / minimum temperature, "hot-case"	+12 / +3°C Observation away from sun	+35 / +30°C Observation away from sun
Battery maximum / minimum temperature, "cold-case"	-6 / -8°C Observation towards sun	+21 / +18°C Observation towards sun
CEU maximum / minimum temperature, "hot-case"	+17 / +10°C Observation away from sun	+38 / +34°C Observation away from sun
CEU maximum / minimum temperature, "cold-case"	0 / -2°C Observation towards sun	+25 / +23°C Observation towards sun
Momentum wheels maximum / minimum temperature, "hot-case"	+16 / +8°C Observation away from sun	+37 / +33°C Observation away from sun
Momentum wheels maximum / minimum temperature, "cold-case"	-1 / -3°C Observation towards sun	+24 / +21°C Observation towards sun

Table 5.5 Electronics results summary

5.3.6 Thermal results discussion

5.3.6.1 Antenna panel thermal discussion

For the antenna panel, the absolute maximum temperature is about 34°C in one of the corner patches, as given in fig. 5.6. This is for side-looking observation towards sun following power generation "mode 1". This occurs at the end of the observation period, and will also be the maximum operating temperature.

The absolute cold temperature is about -78°C in one of the centre patches, as given in fig. 5.12. This is for side-looking observation away from sun following power generation "mode 2". This occurs at the beginning of the observation period, and will also be the minimum operating temperature.

The largest temperature variation on the antenna surface during observation at a given location is about 68°C, as given in fig.5.10. This is for side-looking observation towards sun following power generation “mode 2”.

The largest temperature difference on the antenna surface at a given time during observation, between a corner patch and a centre patch, is about 22°C, as given in figure 5.12. This is for side-looking observation away from sun following power generation “mode 2”.

The largest temperature difference between the front side and the backside of the antenna panel during observation, at a given position and time, is about 15°C at the centre of the panel, comparing end of observation temperatures given in figure 5.10 and 5.11. This is for side-looking observation towards sun following power generation “mode 2”.

The simulations are done with a 15-minute observation time. Some time in each end of this interval is used for changing the satellite attitude from power generation to observation mode and vice versa. The observation period will typically be about 8 minutes. The values for maximum and minimum observation temperatures, taken at each end of the 15-minute interval, are therefore conservative.

The temperature variation across the antenna panel will depend on the conductance of the connection between satellite body and antenna panel. It is necessary to do a more detailed study of the antenna panel mounting in a later study. The conductance values used are given in Appendix D.

5.3.6.2 Bracket thermal discussion

The bracket temperatures given in figure 5.14 and 5.15 shows that the temperature change in the bracket during observation, is mainly on the antenna side. This is due to conduction of heat through the antenna panel/bracket interface, which can be seen when comparing the antenna temperature curves in figure 5.7 and 5.11 with curves 5.14 and 5.15.

The conductance values used for this interface are important for the bracket temperature results, and hence for the thermal-mechanical analyses of the bracket. The values used are conservative, and can be found in Appendix D. It is necessary to do a more detailed study of the antenna panel/bracket interface in a later study.

5.3.6.3 Star tracker and radiator thermal discussion

The star tracker maximum temperature is about -5°C, as given in figure 5.16. This is for target-pointing observation following power generation “mode 1”. The star tracker minimum temperature is about -23°C, as given in fig.5.17. This is for side-looking observation away from the sun following power generation “mode 1”. The largest temperature variation during an orbit is about 8°C, as given in figure 5.16.

According to the requirements specification, the star tracker operating temperature shall be between –35 and +10°C, which is achieved. Maximum temperature variation during an orbit must be within 4°C. For power generation "mode 1", the 4°C maximum ΔT requirement is not achieved, with a ΔT result of 8°C. Due to the varying albedo and IR loads on the radiator in this mode, this requirement seems hard to fulfil. Anyway the maximum ΔT during observation, when high pointing accuracy is necessary, is about 2°C. The ΔT of 8°C is therefore not considered critical.

The radiator area needed in power generation "mode 1" is 365 cm^2, and for power generation "mode 2" the area is 182 cm^2.

5.3.6.4 Solar panels thermal discussion

The solar panel temperatures will vary between –78 and +119°C for power generation "mode 1", and between –77 and +110 for power generation "mode 2". For 94% of the time used for power generation, the temperatures will vary between +80 and +119°C. 119°C is somewhat high with respect to maximum efficiency. The solar panels are thermally and mechanically loose coupled to the satellite structure. To lower the temperatures, either the surface coating (α and ε values) of the solar panels must be changed, or the conductance of the solar panel to satellite body couplings must be increased. However the solar panel temperatures are within typical limits given in the literature [8].

5.3.6.5 Electronics thermal discussion

The electronics temperatures vary between –8 and +17°C for power generation "mode 1", and between +15 and +38°C for power generation "mode 2".

The electronics are only approximately modelled. For some of the boxes it is only estimated what power they will use, how they are connected to their decks, and what heat capacity they have. This approximate model was optimised for power generation "mode 2". The temperatures for power generation "mode 1" are therefore low. This can be solved using connections with lower conductance.

More important is that the temperatures are quite stable during an orbit. All electronics, including the battery will experience an orbital ΔT less than 10°C. For the battery, power generation "mode 1" gives a ΔT of 9°C, and power generation "mode 2" gives a ΔT of 5°C. Deck 2 has more stable temperatures than deck1, and it might be a good idea to place the battery on this deck.

There should be no problem to achieve a temperature environment for the electronics that is well within typical requirements for a spacecraft [8] with this design. A more detailed study of the electronics and their connections to respective decks belongs in a later study.

6 THERMAL-MECHANICAL ANALYSES

6.1 Bracket angular variation

6.1.1 Bracket thermal-mechanical model and analyses

When switching from power generation to side-looking observation towards the sun, the antenna panel is switching from seeing dark space in both power generation modes, to see almost directly into the sun under observation. The temperature gradient in the bracket due to conduction through the antenna/bracket interface will be at its maximum at this time.

Since the high thermal stability of the bracket is required only during observation, we need to find the largest ΔT for the bracket during this period. This has to be done for both power generation modes. The temperatures have a smooth distribution at any time of the orbit, with temperatures being equal around the circumference at a given axial position in the bracket. It is therefore likely that the largest ΔT will also give the largest thermal expansions. The temperatures at each flange on the bracket are shown in figures 5.14 and 5.15. As expected, the largest temperature variations are found at the antenna side. The "cold-case" will occur at the beginning of observation, and the "hot-case" will occur at the end of the observation period. This is also as expected with respect to the antenna loads.

The "hot"- and "cold-case" temperature distributions on the bracket, the spacer and the mounting ring, are shown in figures 6.1 to 6.4. From these thermal results, hot and cold temperature load-fields are created for use in the thermal-mechanical analysis.

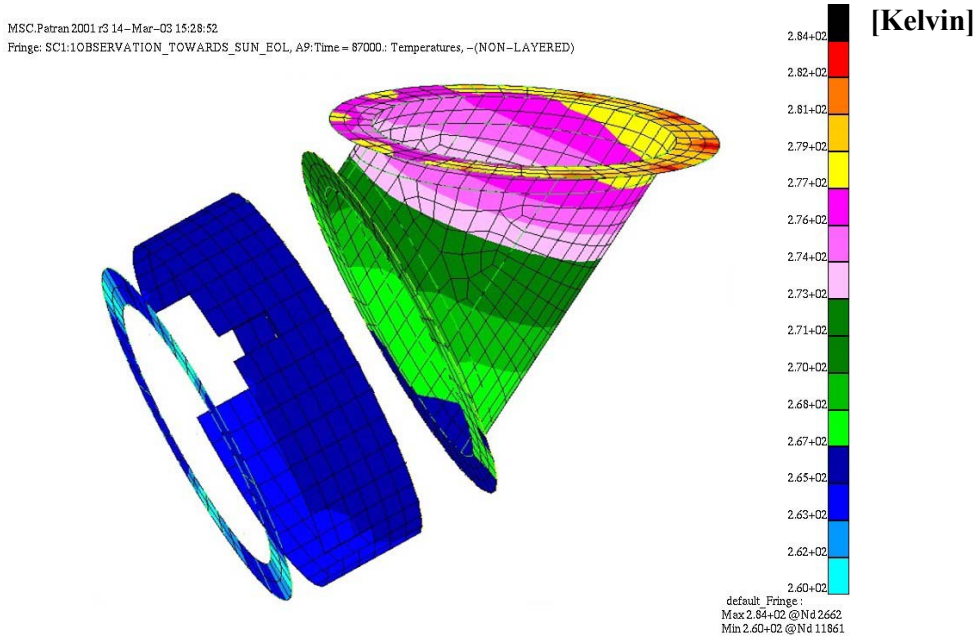

Figure 6.1 Bracket "hot-case" temperatures for side-looking observation towards sun, power generation "mode 1", t=5800 sec.

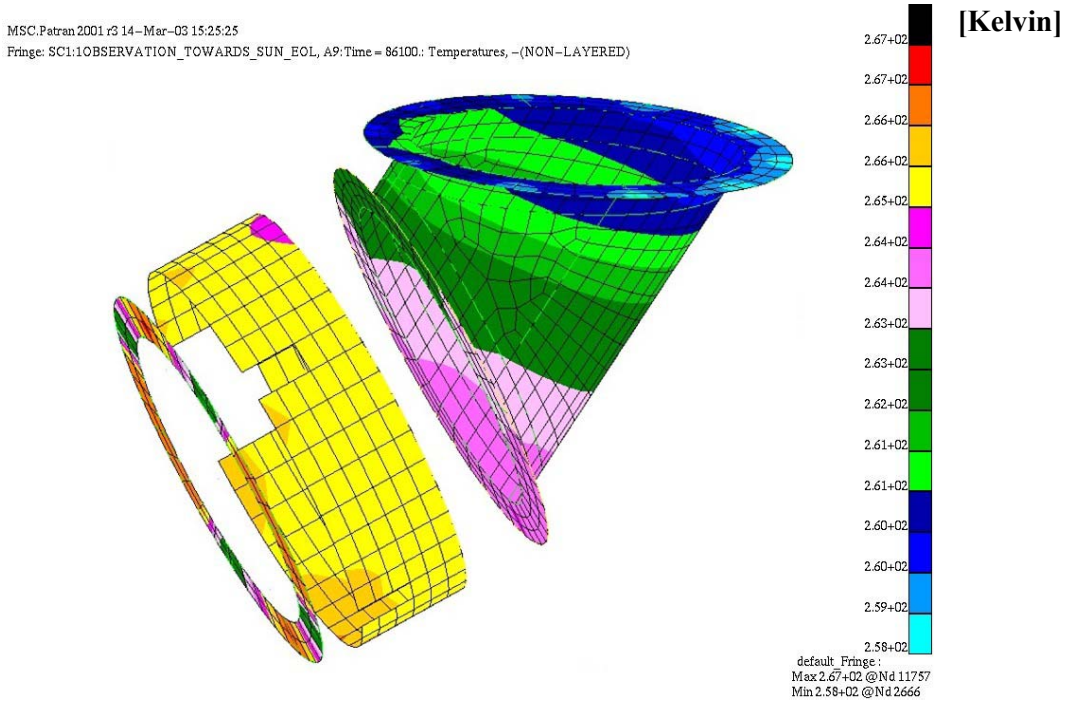

Figure 6.2 Bracket "cold-case" temperatures for side-looking observation towards sun, power generation "mode 1", t=4900 sec.

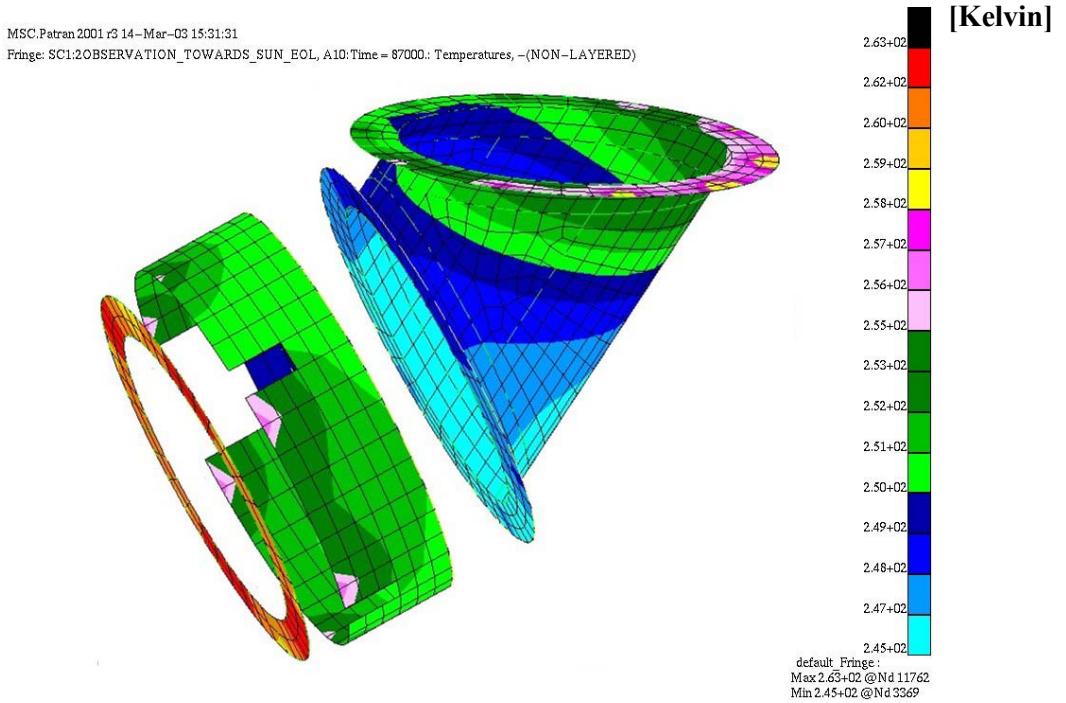

Figure 6.3 Bracket "hot-case" temperatures for side-looking observation towards sun, power generation "mode 2", t=5800 sec.

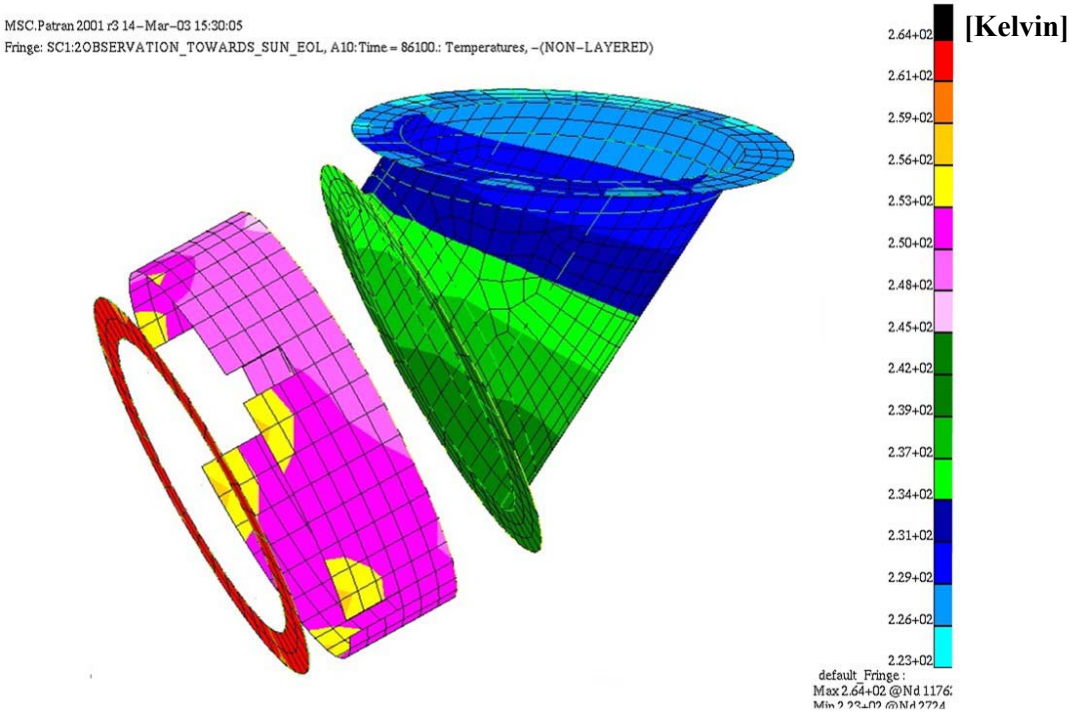

Figure 6.4 Bracket "cold-case" temperatures for side-looking observation towards sun, power generation "mode 2", t=4900 sec.

A new mechanical analysis is run on the bracket, including the spacer and the mounting ring. The "cold-case" temperature distribution from the thermal analysis is set as initial temperature, and the "hot-case" temperature distribution is used as temperature load. It is assumed that the bracket is calibrated at the beginning of the 15-miniute observation period, at the time of the "cold-case". Then the angular variation is gradually increasing until the end of observation, at the time of the "hot-case". Therefore the variation found is not a +/- value, but a total value. The bracket is fixed at the antenna side interface, only allowed to expand in radial direction.

6.1.2 Bracket thermal-mechanical results and discussion

The deformation out of the star tracker interface plane is shown in figure 6.5 for power generation "mode 1", and in figure 6.6 for power generation "mode 2". The bracket stability is calculated from the deformations in the four star tracker mounting points on the mounting ring. The bracket stability is defined as the variation of the angle between the normal of the best fitted plane through the four star tracker mounting points, and the normal of the mounting-flange-plane.

The total angular variation during observation in the bracket is given in table 6.1. These results alone are within the requirement of 1.0 E-3 deg, but the deformations in the star tracker housing and the antenna panel must also be added to the bracket results. The total angular variation is discussed in the conclusion.

	Power generation "mode 1"	**Power generation "mode 2"**
Angular variation in bracket	6.34 E-4 deg	8.74 E-4

Table 6.1 Angular variation in the bracket

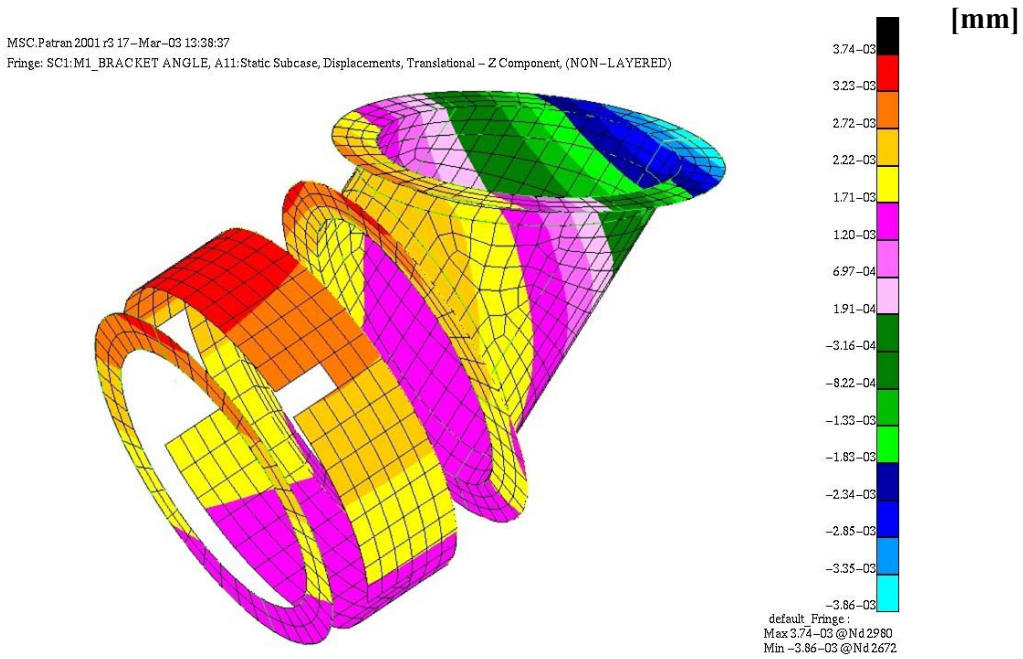

Figure 6.5 Deformations normal to star tracker mounting flange for power generation mode1.

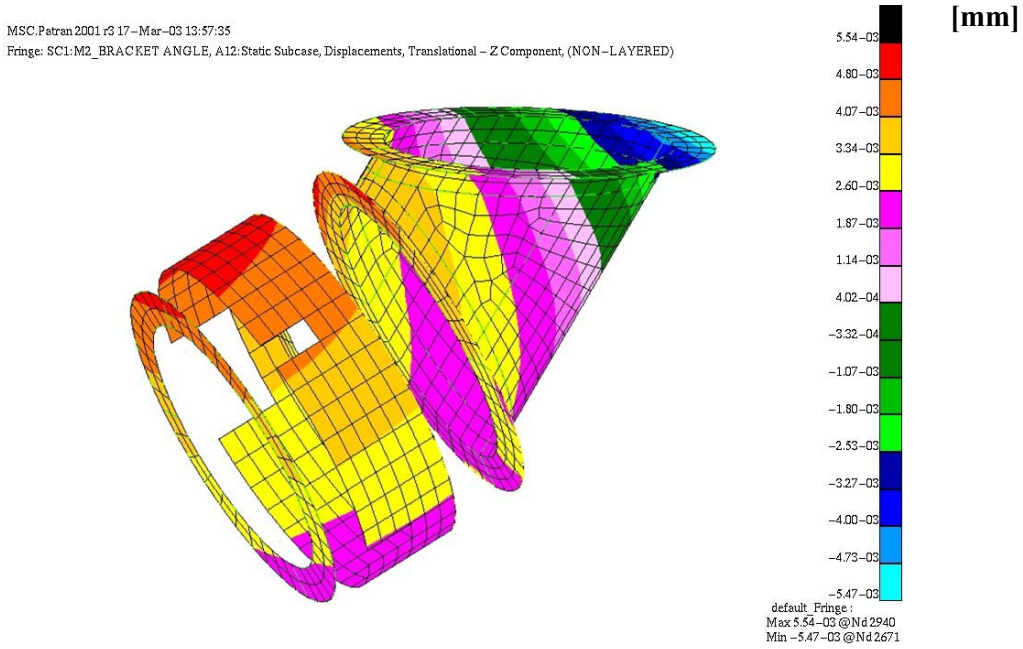

Figure 6.6 Deformations normal to star tracker mounting flange for power generation mode2.

6.2 Antenna flatness

6.2.1 Antenna thermal-mechanical model and analyses

As for the bracket, there are also requirements to the thermal-mechanical stability of the antenna panel. The requirements are set with respect to in-plane deformation, and out-of-plane deformation. Also the antenna panel deformation contributes to the total angular variation between the optical axis of the star tracker and the antenna boresight.

Since the high thermal stability of the antenna panel is required only during observation, we need to find the largest ΔT for the antenna during this period. This has to be done for both power generation modes. The antenna panel is assumed to be perfectly flat at an initial temperature of 20° C. As seen from figures 5.6 to 5.13, the largest ΔT with respect to the initial temperature, will be for the antenna panel "cold-cases" at beginning of observation. "Cold-case" temperatures for both power generation modes at t = 4900 seconds, are shown in figures 6.7 and 6.8. From these thermal results, temperature load-fields are created for use in the thermal-mechanical analysis.

The antenna panel edges at the front of the panel are fixed normal to the antenna-plane, and free to expand in the plane. One corner is fixed.

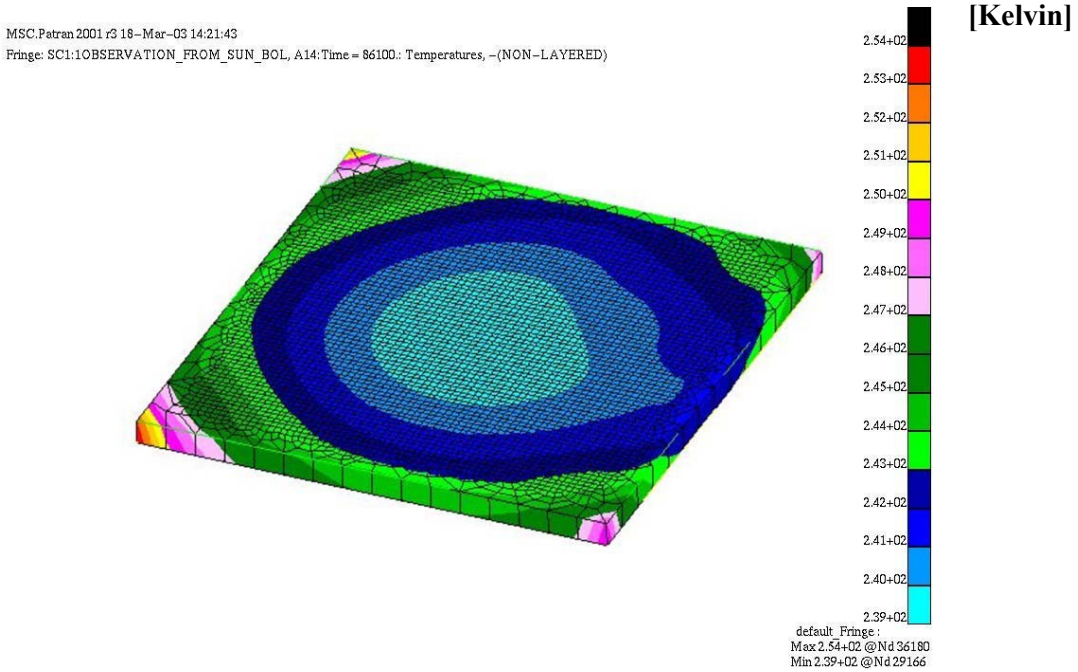

Figure 6.7 Antenna "cold-case" temperatures for side-looking observation away from sun, power generation "mode 2".

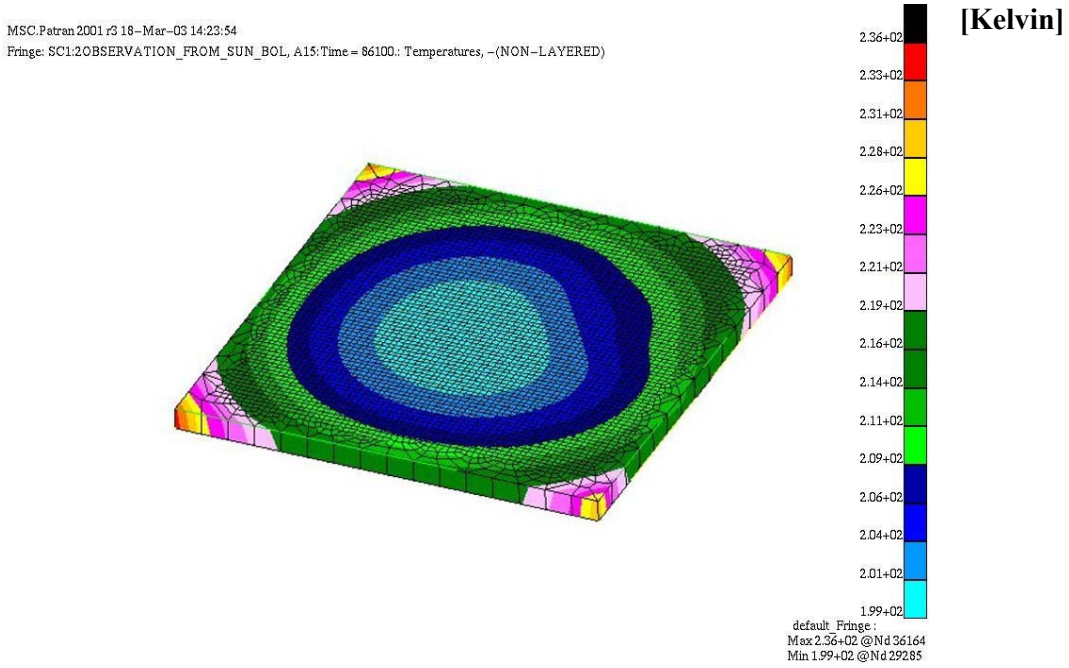

Figure 6.8 Antenna "cold-case" temperatures for side-looking observation away from sun, power generation "mode 2".

6.2.2 Antenna thermal-mechanical results and discussion

The antenna deformations are given in table 6.2.

	Power generation "mode 1"	**Power generation "mode 2"**
Antenna out-of-plane deformations	+1.20µm / - 2.00µm (Ref. fig. 6.9)	+2.26µm / - 2.91µm (Ref. fig. 6.12)
Antenna in-plane deformations along the long/short edge	+161µm / + 148µm (Ref. fig. 6.10)	+242µm / - 220µm (Ref. fig. 6.13)
Antenna through thickness deformations	38 µm (Ref. fig. 6.11)	66 µm (Ref. fig. 6.14)

Table 6.2 Antenna panel deformations.

This is all well within the requirements [18]:

- Out-of-plane maximum deformation between phase centres: Δ = 10µm.
- In-plane maximum deformation between phase centres: $\Delta = \pm$ 1500µm.
- Through plane maximum thickness change: Δ = 80µm.

The 4 phase centres are located on the diagonals, 12.5 cm along each edge of the patch pattern, measured from each 4 corner patches towards the centre of the panel.

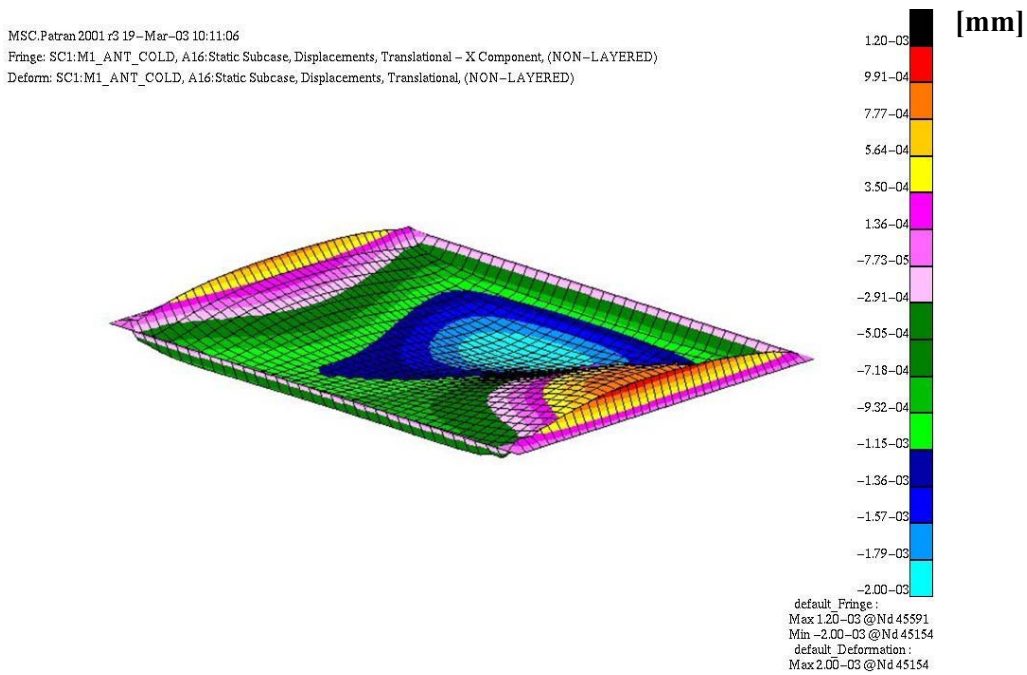

Figure 6.9 Antenna panel surface maximum out-of-plane deformations during observation, power generation "mode 1".

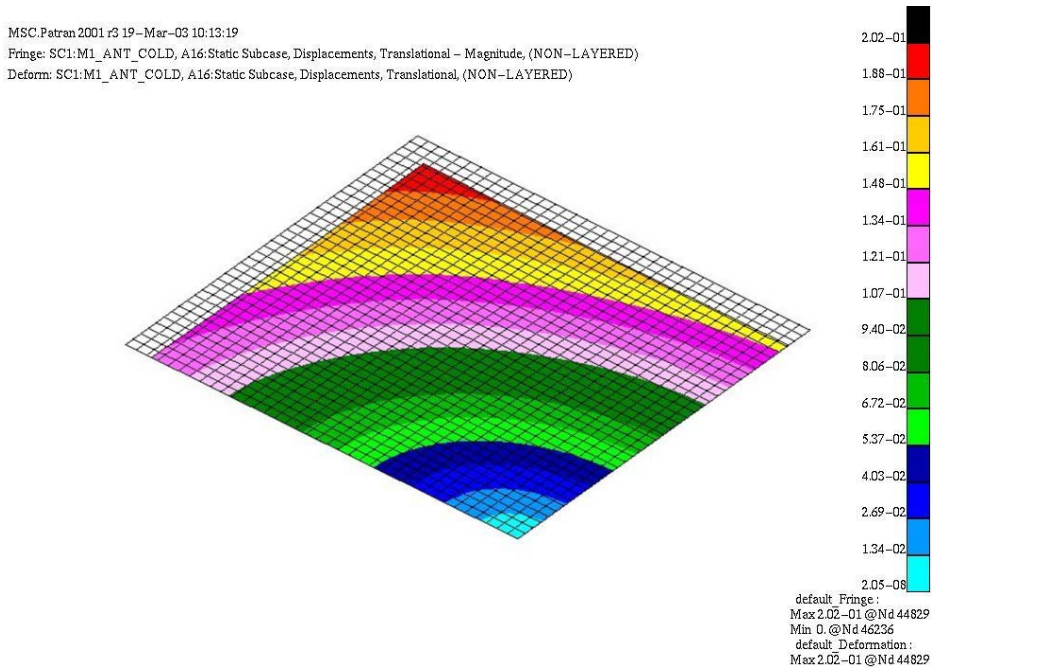

Figure 6.10 Antenna panel surface maximum in-plane deformations during observation, power generation "mode 1".

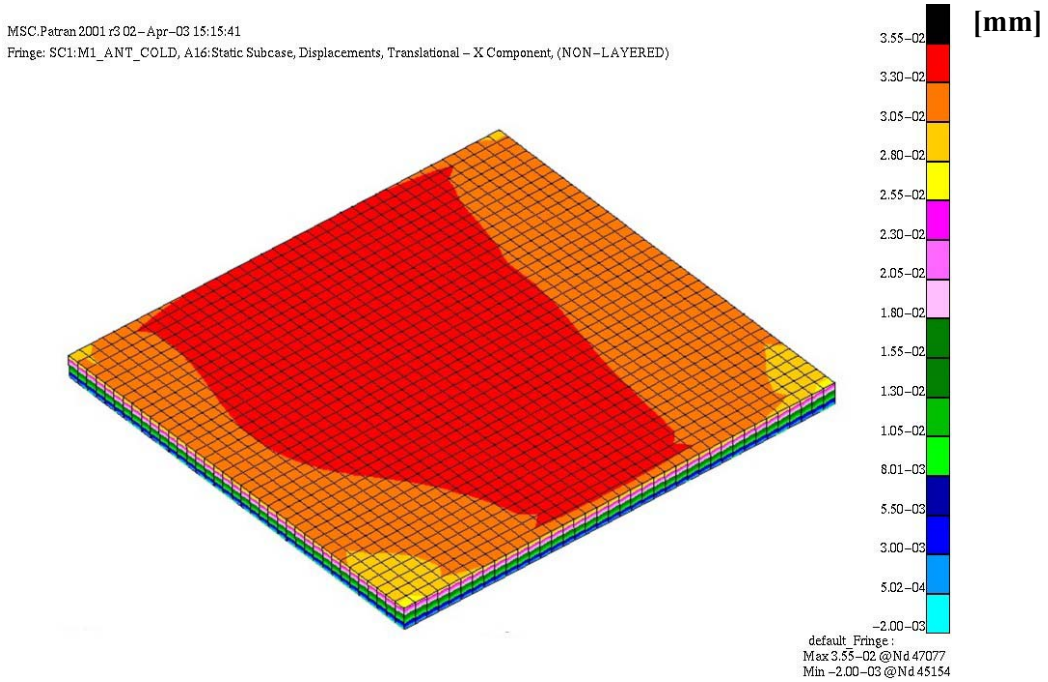

Figure 6.11 Antenna panel through thickness deformation during observation, power generation mode (the backside is being plane).

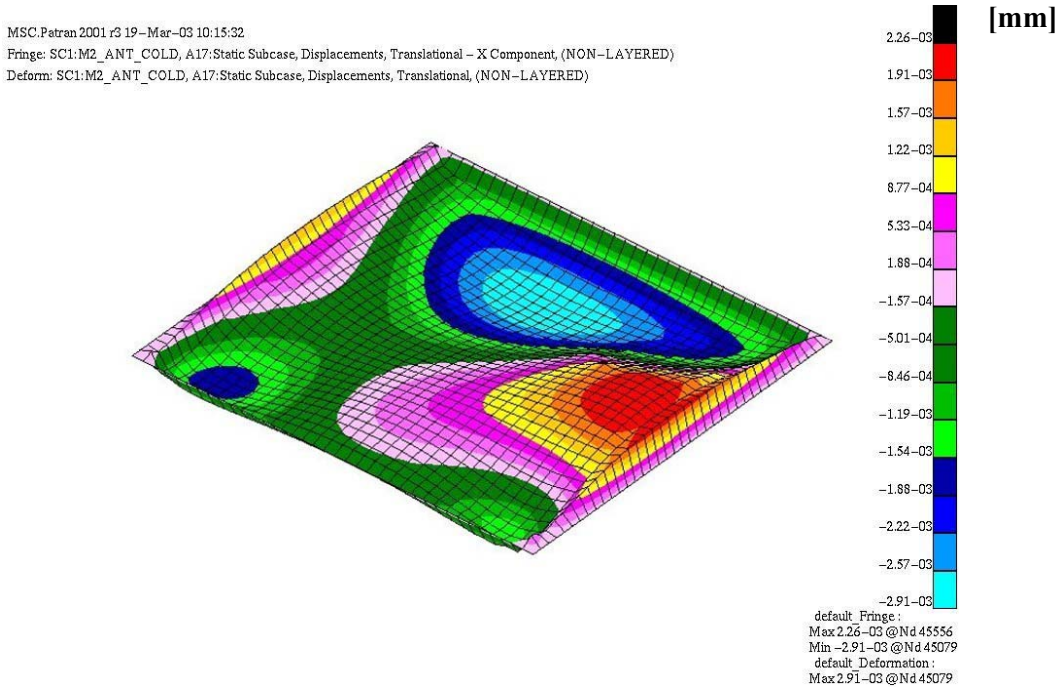

Figure 6.12 Antenna panel surface maximum out-of-plane deformations during observation, power generation "mode 2".

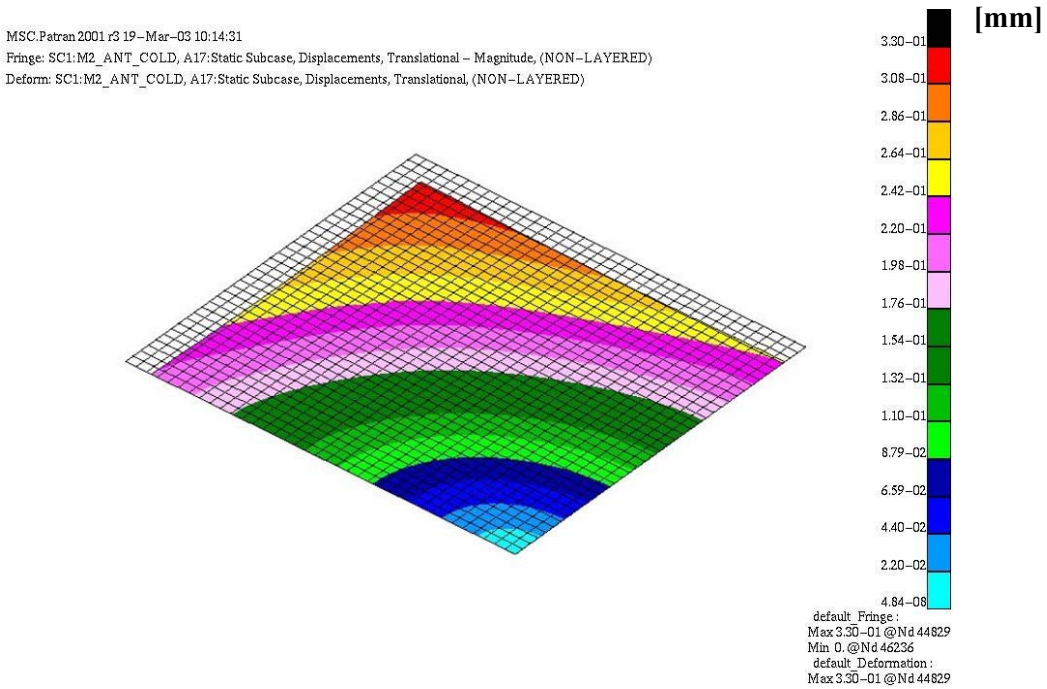

Figure 6.13 Antenna panel surface maximum in-plane deformations during observation, power generation "mode 2".

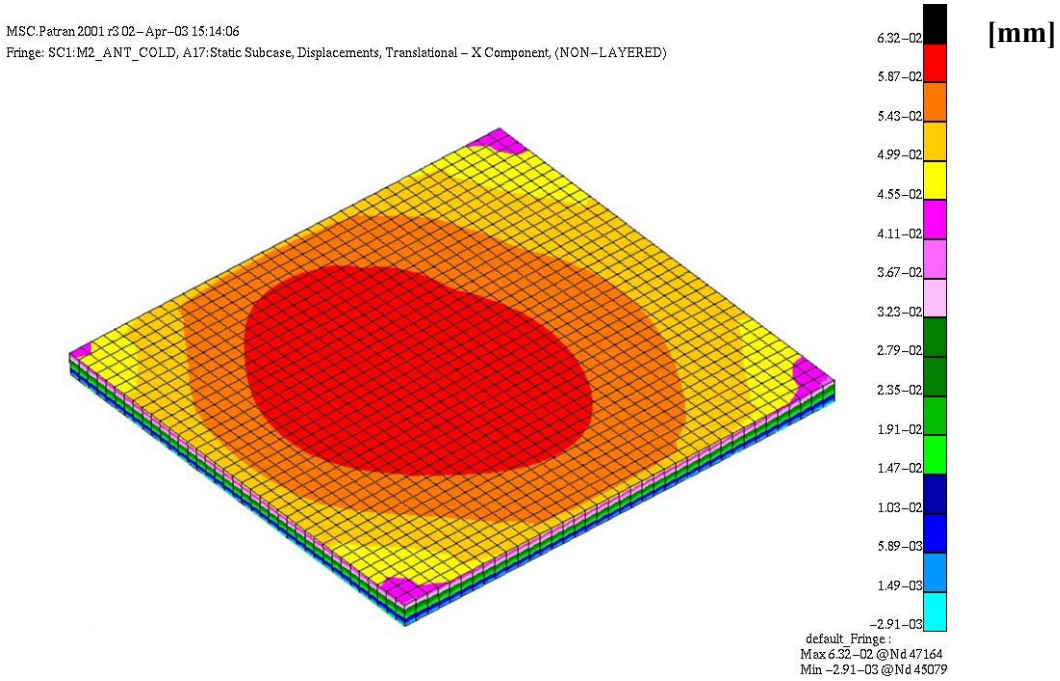

Figure 6.14 Antenna panel through thickness deformation during observation, power generation "mode 2" (the backside is being plane).

The angular variation between the optical axis of the star tracker and the antenna boresight due to deformation of the antenna panel is calculated from out-of-plane deformations of the antenna panel. This angular contribution is measured between the normal of the best fitted plane through the bracket mounting interface at the antenna panel backside, and the normal of the best fitted plane through the four phase centres at the antenna panel front side (the boresight). The antenna panel angular contribution during observation are calculated both for the antenna "cold-case" deformations for side-looking observation away from sun, and for the antenna "hot-case" deformations for side-looking observation towards the sun (not shown here).

The results are:

- "Cold-case", power generation "mode 1": 0.82 E-3 deg
- "Cold-case", power generation "mode 2": 2.87 E-3 deg
- "Hot-case", power generation "mode 1": 1.81 E-3 deg
- "Hot-case", power generation "mode 2": 3.55 E-3 deg

This is not within the intended requirements of 1.0 E-3 deg. However the antenna panel is not subject to a detailed study, and no effort is set to create a more stable panel. Still this gives an indication on the angular contribution of the antenna panel. Both a different layup of the skins, and the use of a core with lower CTE, like carbon composite, might improve the results significantly. Another solution would be to redesign the bracket to be connected to the antenna panel directly at the four phase centers. This would minimize the angular variation between the optical axis of the star tracker and the antenna boresight due to deformation in the antenna panel. However this will result in a more complicated bracket design.

7 CONCLUSIONS

It is critical for the NSAT-1 sensor concept to ensure an extreme thermal-mechanical stability of the observation system. Angular variations between the optical axis of the star tracker and the antenna boresight must be kept as small as possible. Any variation of this angle is due to thermal deformations in the star tracker housing, in the bracket connecting the star tracker to the backside of the antenna panel, and in the antenna panel itself.

To maintain thermal stability the bracket can be made of a winded carbon fibre composite tube. When utilizing the CTE-properties of a typical carbon fibre, and optimizing the fibre layup, the bracket is very stable with respect to thermal-mechanical deformations. The thermal contact resistance at the bracket/antenna interface is essential for the temperature variations, and hence the deformations, experienced by the bracket. Conservative values are used, and more precise ones should be found in later studies. Total angular variation in the bracket during observation is about 0.6 E-3 deg for power generation "mode 1", and about 0.9 E-3 deg for power generation "mode 2".

The optimum mounting location of the bracket relative to the antenna phase centres must be evaluated. A redesign where the bracket is connected directly at the four phase centers would minimize the angular variation between the optical axis of the star tracker and the antenna boresight due to deformation in the antenna panel. However this will result in a more complicated bracket design.

The preliminary antenna panel used in this study consists of an aluminium honeycomb core with carbon fibre composite skins. The results show that the thermal-mechanical stability of the antenna panel is within the requirements with respect to out-of-plane-, in-plane- and through thickness deformations. The antenna panel contribution to the angle between the optical axis of the star tracker and the antenna boresight is significant, and about 3 times the contribution from the bracket. The antenna panel is not subject to a detailed study, and there is clearly room for improvement. A contribution after improvement about the same size as for the bracket seems realistic. Still it can be concluded that the antenna panel thermal mechanical stability is of significant importance to the variations in the total angle between the optical axis of the star tracker and the antenna boresight, as long as the bracket is not connected directly at the four phase centers.

More detailed analyses of the antenna panel and its mounting to the satellite body must be done.

According to the results revealed in this report it is concluded that the requirement of 1.0 E-3 deg maximum variation of the angle between the optical axis of the star tracker and the antenna boresight, cannot be fulfilled. The star tracker itself will take about 0.7 E-3 deg [3] and [19]. The components (bracket, spacer and mounting ring) connecting the star tracker to the backside of the antenna will need about 0.9 E-3 deg. The antenna panel itself has room for improvement but is assumed to need at least 1.0 E-3 deg if the bracket is not redesigned to be connected directly at the four phase centres. The requirement should be revised, giving room for at least a total angular variation between the optical axis of the star tracker and the antenna boresight of 3.0 E-3 deg. Still this is a very strict requirement. Although this could theoretically be achieved, it is recommended to build a prototype of the bracket and the structural antenna panel for real tests.

The solar panels temperatures are within typical limits for spacecraft applications. Temperatures in the electronics are stable, but in general a little to low for power generation “mode 1”. This can easily be adjusted, and is not considered as a problem.

The star tracker temperatures are within the limits during observation. For power generation “mode 1”, the ΔT requirement will fail by 4°C outside the observation period. This is not assumed critical.

Power generation “mode 1” will require a radiator twice as big as for power generation “mode 2”. The temperature variations in the star tracker are larger in mode1, but this mode will give

more stable temperatures on the antenna panel and in the bracket. According to the results presented in this report there is no preferred power generation mode from a thermal point of view.

The temperatures in the antenna panel for side-looking observation towards the sun, when the antenna is turned from dark space towards the sun, do not stabilize, but increase with an almost constant rate during the entire observation. Therefore an additional passing in and out of eclipse during observation, which would occur at wintertime in a 06-18 orbit, will not cause larger temperature variations in the antenna panel. The assumption of an 18-06 orbit being preferable with respect to temperature variations, seems not to hold. From a thermal point of view it is assumed that a 06-18 orbit will give about the same results.

In general, the results show that the NSAT-1 could be realized from a thermal-mechanical point of view. However the requirement of 1.0 E-3 deg maximum variation of the angle between the optical axis of the star tracker and the antenna boresight are too strict, and must be negotiated in the total error budget.

8 FURTHER WORK

Further attention must be paid to the antenna panel and how it is mounted to the satellite structure. It would be of interest to compare the honeycomb panel analysed in this report with the antenna panel from a parallel study initiated by Ericsson AS in cooperation with COI (Composite Optics Inc.) [17].

The bracket mounting to the antenna panel must be further investigated. It is essential to ensure that the expansions of the antenna panel and the bracket do not conflict at the mounting interface. The optimum mounting location of the bracket relative to the phase centres must be evaluated. Also a redesign where the bracket is connected directly at the four phase centers should be considered. More accurate values for the thermal contact resistance at the bracket/antenna interface should be established by experiments or detailed FE-analyses.

To verify the results of the thermal-mechanical bracket analyses, an actual bracket should be built and tested. FFI has the necessary equipment for carbon fibre filament winding and curing. A method for measuring very small angular deformations in the bracket must be established.

Appendix

A LOADCASES

Antenna pointing towards sun, EOL:

Application region	**View Factor (Exposure) Mode 1**	**View factor (Exposure) Mode 2**	**Applied heat**	**Radiation Ambient Temp.**	**Surface props.**	**Duration [s]**
Antenna	Fs_ant	1.0		4 K	$\varepsilon = 0.88$	0 - 4900
Antenna	Fs_ant	0.52		4 K	$\varepsilon = 0.88$	4900 - 5800
Antenna	Fe_ant	0.48		273 K	$\varepsilon = 0.88$	4900 - 5800
Antenna	Fe_ant		AL: View factor · Albedo Function		$\alpha = 0.44$	1450-4350
Antenna	Fe_ant	0.48	IR: View factor ·167 W/m^2		$\alpha = 0.88$	0 - 5800
Antenna	Sin 75.7°	Sin 75.7°	SUN: 1353·sin 75.7 = 1311 W/m^2		$\alpha = 0.44$	4900 - 5800
Bottom / Deck 1 (-x)	Fs_-x	0.18		4 K	$\varepsilon = 0.86$	0 - 4900
Bottom / Deck 1 (-x)	Fe_-x	0.82		273 K	$\varepsilon = 0.86$	0 - 4900
Bottom / Deck 1 (-x)	Fs_-x	0.75		4 K	$\varepsilon = 0.86$	4900 - 5800
Bottom / Deck 1 (-x)	Fe_-x	0.25		273 K	$\varepsilon = 0.86$	4900 - 5800
Bottom / Deck 1 (-x)	Fe_-x	0.81	AL: View factor · Albedo Function		$\alpha = 0.58$	1450-4350
Bottom / Deck 1 (-x)	Fe_-x	0.82	IR: View factor ·218 W/m^2		$\alpha = 0.86$	0 - 4900
Bottom / Deck 1 (-x)	Fe_-x	0.25	IR: View factor ·218 W/m^2		$\alpha = 0.86$	4900 - 5800
Large solar panel (-z)	Fs_-z	0.75		4 K	$\varepsilon = 0.85$	0 - 4900
Large solar panel (-z)	Fe_-z	0.25		273 K	$\varepsilon = 0.85$	0 - 4900
Large solar panel (-z)	Fs_-z	1.0		4 K	$\varepsilon = 0.85$	4900 - 5800
Large solar panel (-z)	Fe_-z	0.21	AL: View factor · Albedo Function		$\alpha = 0.92$	1450 - 4350
Large solar panel (-z)	Fe_-z	0.25	IR: View factor ·218 W/m^2		$\alpha = 0.85$	0 - 4900
Large solar panel (-z)	Sin50°	Sin50°	SUN: 1353·sin50- Q_{el} = 943 W/m^2		$\alpha = 0.92$	0 - 4900
Baffle (-z)	Fs_-z	0.75		4 K	$\varepsilon = 0.82$	0 - 4900
Baffle (-z)	Fe_-z	0.25		273 K	$\varepsilon = 0.82$	0 - 4900
Baffle (-z)	Fs_-z	1.0		4 K	$\varepsilon = 0.82$	4900 - 5800
Baffle (-z)	Fe_-z	0.21	AL: View factor · Albedo Function		$\alpha = 0.53$	1450 - 4350
Baffle (-z)	Fe_-z	0.25	IR: View factor ·218 W/m^2		$\alpha = 0.82$	0 - 4900
Baffle (-z)	Sin50°	Sin50°	SUN: 1353·sin50 =1036 W/m^2		$\alpha = 0.53$	0 - 4900
Small solar panel (-y)	Fs_+y	0.75		4 K	$\varepsilon = 0.85$	0 - 5800
Small solar panel (-y)	Fe_+y	0.25		273 K	$\varepsilon = 0.85$	0 - 5800
Small solar panel (-y)	Fe_+y	0.22	AL: View factor · Albedo Function		$\alpha = 0.92$	1450 - 4350
Small solar panel (-y)	Fe_+y	0.25	IR: View factor ·218 W/m^2		$\alpha = 0.85$	0 - 5800
Small solar panel (-y)	Sin40°	Sin40°	SUN: 1353·sin40- Q_{el} =791 W/m^2		$\alpha = 0.92$	0 - 4900
Short side (+z)	Fs_+z	0.75		4 K	$\varepsilon = 0.30$	0 - 4900
Short side (+z)	Fe_+z	0.25		273 K	$\varepsilon = 0.30$	0 - 4900

Short side (+z)	Fe_+z	0.82		273 K	$\varepsilon = 0.30$	4900 - 5800
Short side (+z)	Fs_+z	0.18		4 K	$\varepsilon = 0.30$	4900 - 5800
Short side (+z)	Fe_+z	0.30	AL: View factor · Albedo Function		$\alpha = 0.30$	1450 - 4350
Short side (+z)	Fe_+z	0.25	IR: View factor ·218 W/m^2		$\alpha = 0.30$	0 - 4900
Short side (+z)	Fe_+z	0.82	IR: View factor ·218 W/m^2		$\alpha = 0.30$	4900 - 5800
Side panel (+y)	Fs_-y	0.75		4 K	$\varepsilon = 0.30$	0 - 5800
Side panel (+y)	Fe_-y	0.25		273 K	$\varepsilon = 0.30$	0 - 5800
Side panel (+y)	Fe_-y	0.28	AL: View factor · Albedo Function		$\alpha = 0.30$	1450 - 4350
Side panel (+y)	Fe_-y	0.25	IR: View factor ·218 W/m^2		$\alpha = 0.30$	0 - 5800
Radiator (+y)	Fs_-y	0.75		4 K	$\varepsilon = 0.80$	0 - 5800
Radiator (+y)	Fe_-y	0.25		273 K	$\varepsilon = 0.80$	0 - 5800
Radiator (+y)	Fe_-y	0.28	AL: View factor · Albedo Function		$\alpha = 0.15$	1450 - 4350
Radiator (+y)	Fe_-y	0.25	IR: View factor ·218 W/m^2		$\alpha = 0.80$	0 - 5800
CEU (Deck1)			16.33 W			0 - 5800
Mom. Wheels (Deck1)			4 x 3.1 W			0 - 5800
Payload (Deck2)			6.98 W			0 - 5800
GPS (Deck2)			6.0 W			0 - 5800
Mag. meter (Deck2)			0.84 W			0 - 5800
Star Tracker			2.5 W			0 - 5800
Magneto Torquers			3 x 0.30 W			0 - 5800

Table A.1 Antenna pointing towards sun, EOL.

Antenna pointing away from sun, BOL:

Application region	**View Factor (Exposure) Mode 1**	**View factor (Exposure) Mode 2**	**Applied heat**	**Radiation Ambient Temp.**	**Surface props.**	**Duration [s]**
Antenna	Fs_ant	1.0		4 K	$\varepsilon = 0.88$	0 - 4900
Antenna	Fs_ant	0.52		4 K	$\varepsilon = 0.88$	4900 - 5800
Antenna	Fe_ant	0.48		273 K	$\varepsilon = 0.88$	4900 - 5800
Antenna	Fe_ant		AL: View factor · Albedo Function		$\alpha = 0.23$	1450-4350
Antenna	Fe_ant	0.48	IR: View factor ·167 W/m^2		$\alpha = 0.88$	0 - 5800
Bottom / Deck 1 (-x)	Fs_-x	0.18		4 K	$\varepsilon = 0.86$	0 - 4900
Bottom / Deck 1 (-x)	Fe_-x	0.82		273 K	$\varepsilon = 0.86$	0 - 4900
Bottom / Deck 1 (-x)	Fs_-x	0.75		4 K	$\varepsilon = 0.86$	4900 - 5800
Bottom / Deck 1 (-x)	Fe_-x	0.25		273 K	$\varepsilon = 0.86$	4900 - 5800
Bottom / Deck 1 (-x)	Cos15.4°	Cos15.4°	SUN: 1353·cos15.4 = 1304 W/m^2		$\alpha = 0.58$	4900 - 5800
Bottom / Deck 1 (-x)	Fe_-x	0.81	AL: View factor · Albedo Function		$\alpha = 0.58$	1450-4350
Bottom / Deck 1 (-x)	Fe_-x	0.82	IR: View factor ·218 W/m^2		$\alpha = 0.86$	0 - 4900
Bottom / Deck 1 (-x)	Fe_-x	0.25	IR: View factor ·218 W/m^2		$\alpha = 0.86$	4900 - 5800
Large solar panel (-z)	Fs_-z	0.75		4 K	$\varepsilon = 0.85$	0 - 4900
Large solar panel (-z)	Fe_-z	0.25		273 K	$\varepsilon = 0.85$	0 - 4900
Large solar panel (-z)	Fs_-z	1.0		4 K	$\varepsilon = 0.85$	4900 - 5800
Large solar panel (-z)	Fe_-z	0.21	AL: View factor · Albedo Function		$\alpha = 0.92$	1450 - 4350
Large solar panel (-z)	Fe_-z	0.25	IR: View factor ·218 W/m^2		$\alpha = 0.85$	0 - 4900
Large solar panel (-z)	Sin50°	Sin50°	SUN: 1353·sin50- Q_{el} = 943 W/m^2		$\alpha = 0.92$	0 - 4900
Baffle (-z)	Fs_-z	0.75		4 K	$\varepsilon = 0.82$	0 - 4900
Baffle (-z)	Fe_-z	0.25		273 K	$\varepsilon = 0.82$	0 - 4900
Baffle (-z)	Fs_-z	1.0		4 K	$\varepsilon = 0.82$	4900 - 5800
Baffle (-z)	Fe_-z	0.21	AL: View factor · Albedo Function		$\alpha = 0.53$	1450 - 4350
Baffle (-z)	Fe_-z	0.25	IR: View factor ·218 W/m^2		$\alpha = 0.82$	0 - 4900
Baffle (-z)	Sin50°	Sin50°	SUN: 1353·sin50 =1036 W/m^2		$\alpha = 0.53$	0 - 4900
Small solar panel (-y)	Fs_+y	0.75		4 K	$\varepsilon = 0.85$	0 - 5800
Small solar panel (-y)	Fe_+y	0.25		273 K	$\varepsilon = 0.85$	0 - 5800
Small solar panel (-y)	Fe_+y	0.22	AL: View factor · Albedo Function		$\alpha = 0.92$	1450 - 4350
Small solar panel (-y)	Fe_+y	0.25	IR: View factor ·218 W/m^2		$\alpha = 0.85$	0 - 5800
Small solar panel (-y)	Sin40°	Sin40°	SUN: 1353·sin40- Q_{el} =791 W/m^2		$\alpha = 0.92$	0 - 4900
Short side (+z)	Fs_+z	0.75		4 K	$\varepsilon = 0.30$	0 - 4900
Short side (+z)	Fe_+z	0.25		273 K	$\varepsilon = 0.30$	0 - 4900
Short side (+z)	Fe_+z	0.82		273 K	$\varepsilon = 0.30$	4900 - 5800
Short side (+z)	Fs_+z	0.18		4 K	$\varepsilon = 0.30$	4900 - 5800
Short side (+z)	Fe_+z	0.30	AL: View factor · Albedo Function		$\alpha = 0.30$	1450 - 4350
Short side (+z)	Fe_+z	0.25	IR: View factor ·218 W/m^2		$\alpha = 0.30$	0 - 4900

Short side (+z)	Fe_+z	0.82	IR: View factor ·218 W/m^2		α = 0.30	4900 - 5800
Side panel (+y)	Fs_-y	0.75		4 K	ε = 0.30	0 - 5800
Side panel (+y)	Fe_-y	0.25		273 K	ε = 0.30	0 - 5800
Side panel (+y)	Fe_-y	0.28	AL: View factor · Albedo Function		α = 0.30	1450 - 4350
Side panel (+y)	Fe_-y	0.25	IR: View factor ·218 W/m^2		α = 0.30	0 - 5800
Radiator (+y)	Fs_-y	0.75		4 K	ε = 0.80	0 - 5800
Radiator (+y)	Fe_-y	0.25		273 K	ε = 0.80	0 - 5800
Radiator (+y)	Fe_-y	0.28	AL: View factor · Albedo Function		α = 0.09	1450 - 4350
Radiator (+y)	Fe_-y	0.25	IR: View factor ·218 W/m^2		α = 0.80	0 - 5800
CEU (Deck1)			16.33 W			0 - 5800
Mom. Wheels (Deck1)			4 x 3.1 W			0 - 5800
Payload (Deck2)			6.98 W			0 - 5800
GPS (Deck2)			6.0 W			0 - 5800
Mag. meter (Deck2)			0.84 W			0 - 5800
Star Tracker			2.5 W			0 - 5800
Magneto Torquers			3 x 0.30 W			0 - 5800

Table A.2 Antenna pointing away from sun, BOL.

Target pointing antenna, EOL:

Application region	**View Factor (Exposure) Mode 1**	**View Factor (Exposure) Mode 2**	**Applied heat**	**Radiation Ambient Temp.**	**Surface props.**	**Duration [s]**
Antenna	Fs_ant	1.0		4 K	$\varepsilon = 0.88$	0 - 4900
Antenna	Fs_ant	0.52		4 K	$\varepsilon = 0.88$	4900 - 5800
Antenna	Fe_ant	0.48		273 K	$\varepsilon = 0.88$	4900 - 5800
Antenna	Fe_ant		AL: View factor · Albedo Function		$\alpha = 0.44$	1450-4350
Antenna	Fe_ant	0.48	IR: View factor ·167 W/m^2		$\alpha = 0.88$	0 - 5800
Antenna	Fexp_ant	Fexp_ant	SUN: Exposure factor · 1353 W/m^2		$\alpha = 0.44$	4900 - 5800
Bottom / Deck 1 (-x)	Fs_-x	0.18		4 K	$\varepsilon = 0.86$	0 - 4900
Bottom / Deck 1 (-x)	Fe_-x	0.82		273 K	$\varepsilon = 0.86$	0 - 4900
Bottom / Deck 1 (-x)	Fs_-x	0.75		4 K	$\varepsilon = 0.86$	4900 - 5800
Bottom / Deck 1 (-x)	Fe_-x	0.25		273 K	$\varepsilon = 0.86$	4900 - 5800
Bottom / Deck 1 (-x)	Fe_-x	0.81	AL: View factor · Albedo Function		$\alpha = 0.58$	1450-4350
Bottom / Deck 1 (-x)	Fe_-x	0.82	IR: View factor ·218 W/m^2		$\alpha = 0.86$	0 - 4900
Bottom / Deck 1 (-x)	Fe_-x	0.25	IR: View factor ·218 W/m^2		$\alpha = 0.86$	4900 - 5800
Large solar panel (-z)	Fs_-z	0.75		4 K	$\varepsilon = 0.85$	0 - 4900
Large solar panel (-z)	Fe_-z	0.25		273 K	$\varepsilon = 0.85$	0 - 4900
Large solar panel (-z)	Fs_-z	1.0		4 K	$\varepsilon = 0.85$	4900 - 5800
Large solar panel (-z)	Fe_-z	0.21	AL: View factor · Albedo Function		$\alpha = 0.92$	1450 - 4350
Large solar panel (-z)	Fe_-z	0.25	IR: View factor ·218 W/m^2		$\alpha = 0.85$	0 - 4900
Large solar panel (-z)	Sin50°	Sin50°	SUN: 1353·sin50- Q_{el} = 943 W/m^2		$\alpha = 0.92$	0 - 4900
Baffle (-z)	Fs_-z	0.75		4 K	$\varepsilon = 0.82$	0 - 4900
Baffle (-z)	Fe_-z	0.25		273 K	$\varepsilon = 0.82$	0 - 4900
Baffle (-z)	Fs_-z	1.0		4 K	$\varepsilon = 0.82$	4900 - 5800
Baffle (-z)	Fe_-z	0.21	AL: View factor · Albedo Function		$\alpha = 0.53$	1450 - 4350
Baffle (-z)	Fe_-z	0.25	IR: View factor ·218 W/m^2		$\alpha = 0.82$	0 - 4900
Baffle (-z)	Sin50°	Sin50°	SUN: 1353·sin50 =943 W/m^2		$\alpha = 0.53$	0 - 4900
Small solar panel (-y)	Fs_+y	0.75		4 K	$\varepsilon = 0.85$	0 - 5800
Small solar panel (-y)	Fe_+y	0.25		273 K	$\varepsilon = 0.85$	0 - 5800
Small solar panel (-y)	Fe_+y	0.22	AL: View factor · Albedo Function		$\alpha = 0.92$	1450 - 4350
Small solar panel (-y)	Fe_+y	0.25	IR: View factor ·218 W/m^2		$\alpha = 0.85$	0 - 5800
Small solar panel (-y)	Sin40°	Sin40°	SUN: 1353·sin40- Q_{el} =791 W/m^2		$\alpha = 0.92$	0 - 4900
Short side (+z)	Fs_+z	0.75		4 K	$\varepsilon = 0.30$	0 - 4900
Short side (+z)	Fe_+z	0.25		273 K	$\varepsilon = 0.30$	0 - 4900
Short side (+z)	Fe_+z	0.82		273 K	$\varepsilon = 0.30$	4900 - 5800
Short side (+z)	Fs_+z	0.18		4 K	$\varepsilon = 0.30$	4900 - 5800
Short side (+z)	Fe_+z	0.30	AL: View factor · Albedo Function		$\alpha = 0.30$	1450 - 4350
Short side (+z)	Fe_+z	0.25	IR: View factor ·218 W/m^2		$\alpha = 0.30$	0 - 4900

Short side (+z)	Fe_+z	0.82	IR: View factor ·218 W/m^2		α = 0.30	4900 - 5800
Side panel (+y)	Fs_-y	0.75		4 K	ε = 0.30	0 - 5800
Side panel (+y)	Fe_-y	0.25		273 K	ε = 0.30	0 - 5800
Side panel (+y)	Fexp_-y	Fexp_-y	SUN: Exposure factor ·1353 W/m^2		α = 0.30	4900 - 5800
Side panel (+y)		0.28	AL: View factor · Albedo Function		α = 0.30	1450 - 4350
Side panel (+y)		0.25	IR: View factor ·218 W/m^2		α = 0.30	0 - 5800
Radiator (+y)		0.75		4 K	ε = 0.80	0 - 5800
Radiator (+y)		0.25		273 K	ε = 0.80	0 - 5800
Radiator (+y)	Fexp_-y	Fexp_-y	SUN: Exposure factor ·1353 W/m^2		α = 0.15	4900 - 5800
Radiator (+y)		0.28	AL: View factor · Albedo Function		α = 0.15	1450 - 4350
Radiator (+y)		0.25	IR: View factor ·218 W/m^2		α = 0.80	0 - 5800
CEU (Deck1)			16.33 W			0 - 5800
Mom. Wheels (Deck1)			4 x 3.1 W			0 - 5800
Payload (Deck2)			6.98 W			0 - 5800
GPS (Deck2)			6.0 W			0 - 5800
Magnetometer (Deck2)			0.84 W			0 - 5800
Star Tracker			2.5 W			0 - 5800
Magneto Torquers			3 x 0.30 W			0 - 5800

Table A.3 Target pointing antenna, EOL.

B CREATING VIEW FACTOR CURVES

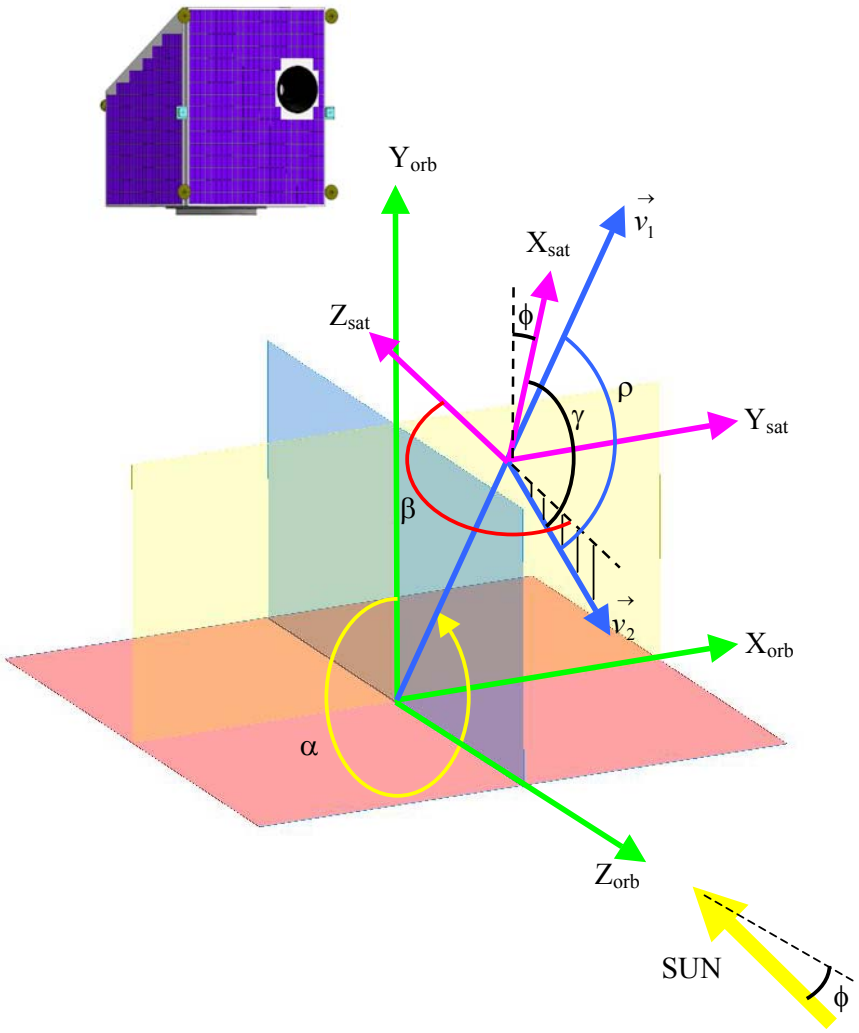

Figure B.1 Orbital- and satellite coordinate systems and their parameters.

Parameters:

- $_{sat}$ = Satellite coordinate system.
- $_{orb}$ = Orbital coordinate system.
- $\vec{v}_1$ = Local zenith normal vector, defined in orbital coordinate system.
- $\vec{v}_2$ = Satellite surface normal vector, defined in satellite coordinate system.
- $\vec{v}_2^*$ = Satellite surface normal vector, transformed into orbital coordinate system.
- α = Angle indicating satellite position in the orbital xy-plane.
- β = Angle between satellite z-axis and satellite surface normal vector, projected into satellite yz-plane.
- γ = Angle between satellite x-axis and satellite surface normal vector, in arbitrary plane normal to satellite yz-plane.

- ϕ = Angle out of the orbital xy-plane between satellite x-axis and orbital y-axis[3].
- ρ = Resulting angle between satellite surface normal vector and local zenith normal vector.

$$\vec{v}_1 = [-\sin\alpha, \cos\alpha, 0] \tag{B.1}$$

$$\vec{v}_2 = [\cos\gamma, -\sin\beta \cdot \sin\gamma, \cos\beta \cdot \sin\gamma] \tag{B.2}$$

Transformation from satellite coordinate system to orbital coordinate system:

$$v_{x\_orb} = v_{y\_sat} \tag{B.3}$$

$$v_{y\_orb} = v_{x\_sat} \cdot \cos\phi + v_{z\_sat} \cdot \sin\varphi \tag{B.4}$$

$$v_{z\_orb} = -v_{z\_sat} \cdot \cos\phi + v_{x\_sat} \cdot \sin\phi \tag{B.5}$$

Transforming $\vec{v}_2$ to orbital coordinate system gives:

$$\vec{v}_2^{*} = [-\sin\beta \cdot \sin\gamma, \cos\gamma \cdot \cos\phi + \cos\beta \cdot \sin\gamma \cdot \sin\phi, -\cos\beta \cdot \sin\gamma \cdot \cos\phi + \cos\gamma \cdot \sin\phi] \tag{B.6}$$

Angle between satellite surface normal vector and local zenith normal vector is found from the scalar product of $\vec{v}_1$ and: $\vec{v}_2^{*}$

$$\vec{v}_1 \bullet \vec{v}_2^{*} = \left|\vec{v}_1\right| \cdot \left|\vec{v}_2^{*}\right| \cdot \cos\rho \tag{B.7}$$

This gives an expression for ρ:

$$\rho = \cos^{-1}\left[\frac{\sin\alpha \cdot \sin\beta \cdot \sin\gamma + \cos\alpha(\cos\gamma \cdot \cos\phi + \cos\beta \cdot \sin\gamma \cdot \sin\phi)}{\sqrt{(-\sin\alpha)^2 + (\cos\alpha)^2} \cdot \sqrt{(-\sin\beta \cdot \sin\gamma)^2 + (\cos\gamma \cdot \cos\phi + \cos\beta \cdot \sin\gamma \cdot \sin\phi)^2 + (-\cos\beta \cdot \cos\phi \cdot \sin\gamma + \cos\gamma \cdot \sin\phi)^2}}\right] \tag{B.8}$$

Equation (B.8) is implemented into an excel worksheet [15]. The ρ-angle is calculated for any α, β, γ and ϕ. Given the diagram in figure B.2 [7], The view factor to earth for any side at any time can be found. The view factor to earth as function of ρ-angle is shown in figure B.3. Together with earth IR values as function of time of year, and albedo values as function of time of year and latitude [7], shown in table B.1 and B.2, complete earth IR and albedo load-curves are created for all sides of the satellite.

[3] The satellite x-axis is always pointing to inertial north during power generation. Given an orbit inclination of 98 deg and an earth tilt of 23.4 deg, the ϕ-angle will vary between +15.4 and –31.4 deg during one year.

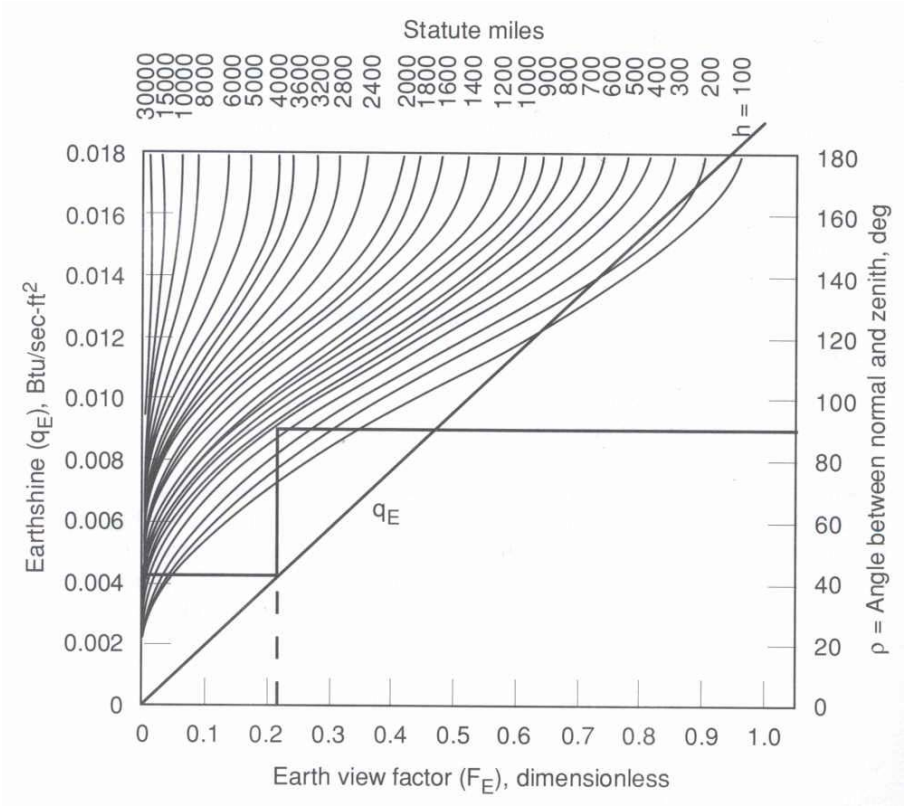

Figure B.2 View factor as function of ρ-angle and orbit altitude.

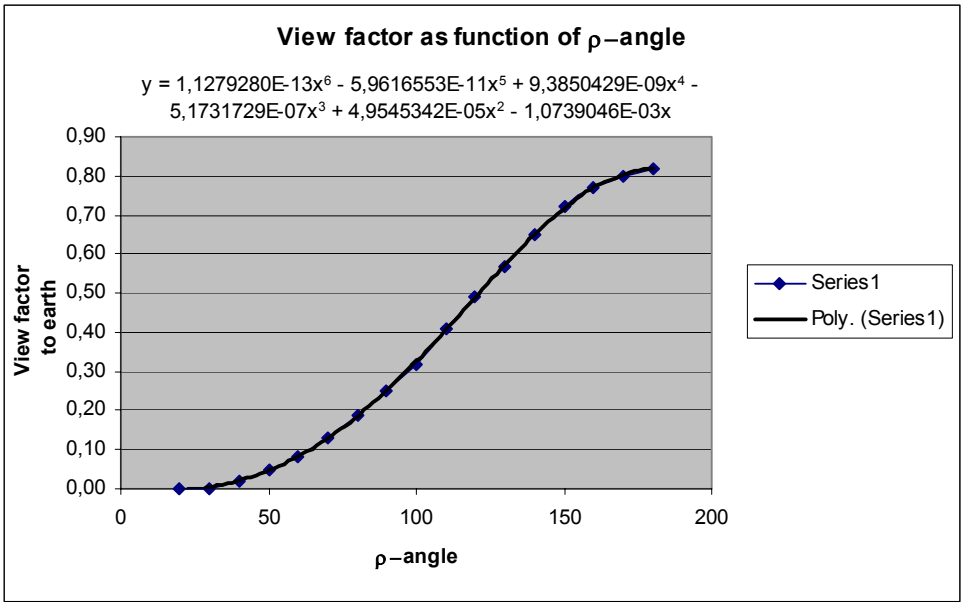

Figure B.3 View factor as function of ρ-angle.

Zonal Mean IR (W/M^2)

Latitude (deg)		Month												Annual		
		J	F	M	A	M	J	J	A	S	O	N	D	Min	Avg	Max
90	80	165	155	146	173	189	207	207	199	178	170	163	177	146	177	207
80	70	157	149	154	183	197	211	212	207	186	175	160	156	149	178	212
70	60	165	164	170	196	208	221	224	217	198	186	173	167	164	190	224
60	50	175	177	188	204	213	222	228	224	211	200	188	182	175	201	228
50	40	191	194	203	216	226	235	244	243	232	220	205	198	191	217	244
40	30	217	218	224	235	241	254	259	263	253	247	231	222	217	238	263
30	20	250	248	251	265	266	268	262	261	261	263	253	251	248	258	268
20	10	266	264	261	270	260	251	241	236	242	250	251	259	236	254	270
10	0	251	251	248	240	232	233	233	235	235	244	242	250	232	241	251
0	-10	240	240	240	243	257	261	261	261	260	257	248	246	240	251	261
-10	-20	248	247	250	264	270	273	272	276	271	266	257	253	247	262	276
-20	-30	261	256	254	263	258	260	260	264	259	258	256	262	254	259	264
-30	-40	253	251	244	239	233	229	231	232	233	238	239	249	229	239	253
-40	-50	232	232	225	217	213	209	205	207	211	219	220	229	205	218	232
-50	-60	217	217	208	204	199	195	188	187	192	201	208	216	187	202	217
-60	-70	209	204	193	186	177	172	164	161	165	180	197	209	161	184	209
-70	-80	196	184	165	153	146	146	131	124	128	151	183	220	124	160	220
-80	-90	187	171	148	121	105	110	104	94	94	126	170	190	94	135	190
	Min	157	149	146	121	105	110	104	94	94	126	160	156			
	Avg	215	212	209	215	216	219	218	216	211	213	213	218			
	Max	266	264	261	270	270	273	272	276	271	266	257	262			

Table B.1 IR as function of latitude.

Zonal Mean Albedo (Percent)

Latitude (deg)		Month												Annual		
		J	F	M	A	M	J	J	A	S	O	N	D	Min	Avg	Max
90	80	80*	78*	69	58	69	75	69	60	44	70*	75*	78*	44	69	80
80	70	81*	83	69	63	62	54	50	49	66	77	77*	80*	49	68	83
70	60	78	56	55	54	49	42	39	40	42	51	64	69	39	53	78
60	50	56	50	49	42	40	39	38	38	37	43	49	55	37	44	56
50	40	46	43	40	36	34	35	33	32	33	34	39	46	32	37	46
40	30	37	36	34	32	30	28	27	26	29	29	33	37	26	31	37
30	20	30	29	27	25	25	25	26	26	26	26	28	30	20	26	30
20	10	24	23	22	20	22	24	26	27	25	25	26	26	25	24	27
10	0	24	24	24	24	26	26	26	26	26	25	26	26	24	25	26
0	-10	25	24	24	24	21	22	23	23	22	23	24	25	21	23	25
-10	-20	24	23	23	22	21	21	22	22	22	23	24	24	21	22	24
-20	-30	23	24	24	23	24	24	25	25	25	25	24	23	23	24	25
-30	-40	27	28	29	29	30	30	30	30	29	29	28	27	27	28	30
-40	-50	33	34	34	37	38	39	39	36	35	34	34	33	33	35	39
-50	-60	41	41	40	42	44	47	48	45	43	44	43	42	40	43	48
-60	-70	46	47	46	54	62	72	77	65	56	56	52	49	46	56	77
-70	-80	61	62	61	86	86*	87*	87*	88	79	65	66	64	61	74	83
-80	-90	70	72	40	80*	81*	82*	82*	83*	80	67	75	75	40	74	83
	Min	23	23	22	20	21	21	22	22	22	23	24	23			
	Avg	45	43	39	41	42	42	42	41	39	41	43	44			
	Max	81	83	69	86	86	87	87	88	80	77	77	78			

* Estimated value

Table B.2 Albedo as function of latitude.

C DATA FOR MECHANICAL MODEL

Radiator and baffle, Al 6082-T6, represented as an isotropic material in MSC.Patran/Nastran [9]:

Modulus of elastisity:	E = 69.0 [GPa]
Poissons ratio:	$\nu = 0.33$
Shear modulus:	G = 26 [GPa]
Density:	$\rho = 2700$ [kg/m^3]

Bracket flanges and mounting ring, Titanium Grade 5, represented as an isotropic material in MSC.Patran/Nastran [9]:

Modulus of elastisity:	E = 113.8 [GPa]
Poissons ratio:	ν = 0.342
Shear modulus:	G = 44 [GPa]
Density:	ρ = 4430 [kg/m$^{3]}$
CTE:	α = 8.6E-6 [/°C]

T-300 carbon fibre composite, 60% fibre and 40% matrix (volume percent), represented as a 2D orthotropic material in MSC.Patran/Nastran:

Composite modulus of elasticity [13]:

In fibre direction: $$E_{11} = V_f \cdot E_{f11} + (1 - V_f) \cdot E_m \quad \text{(C.1)}$$

Normal to fibre direction: $$E_{22} = \frac{1}{\frac{\sqrt{V_f}}{E_{f22} \cdot \sqrt{V_f} + (1 - \sqrt{V_f}) \cdot E_m} + \frac{(1 - V_f)}{E_m}} \quad \text{(C.2)}$$

Composite Coefficients of Thermal Expansion (CTE) [6]:

In fibre direction: $$\alpha_{11} = \frac{E_f \cdot \alpha_{f11} \cdot V_f + E_m \cdot \alpha_m \cdot V_m}{E_f \cdot V_f + E_m \cdot V_m} \quad \text{(C.3)}$$

Normal to fibre direction:

$$\alpha_{22} = \alpha_{f11} \cdot V_f \cdot (1 + \nu_{f12} \cdot \frac{\alpha_{f11}}{\alpha_{f22}}) + \alpha_m \cdot V_m \cdot (1 + \nu_{m12}) - (\nu_{f12} \cdot V_f + \nu_{12m} \cdot V_m) \cdot \alpha_{11} \quad \text{(C.4)}$$

Given carbon fibre and matrix properties [11], [12]:

Modulus of elastisity in fibre direction:	E_{f11} = 221 [GPa]
Modulus of elastisity normal to fibre direction:	E_{f22} = 13.8 [GPa]
Modulus of elastisity for matrix:	E_m = 3.77 [GPa]
Volume fraction of fibre:	V_f = 0.6
Volume fraction of matrix	V_m = 0.4
Density of fibre:	ρ_f =1772 [kg/m^3]
Density of matrix:	ρ_m = 1266 [kg/m^3]
CTE in fibre direction:	α_{f11} = -0.99E-6 [/°C]
CTE normal to fibre direction:	α_{f22} = 10.1E-6 [/°C]
CTE for matrix:	α_m = 60.2E-6 [/°C]

Data inserted into C.1 and C.2, gives modulus of elasticity for unidirectional composite:

Composite modulus of elastisity in fibre direction: E_{11} = 134 [GPa]
Composite modulus of elastisity normal to fibre direction: E_{22} = 7.9 [GPa]

Inserted into C.3 and C.4, gives CTE values unidirectional composite:

Composite CTE in fibre direction: α_{11} = -0.30E-6 [/°C]
Composite CTE normal to fibre direction: α_{22} = 38.5E-6 [/°C]

Composite density for 60 % (Vol.) fibre: ρ_{comp} = 1570 [kg/m^3]

Failure criterion (maximum stress criterion):

Maximum tension in fibre direction: 1300 [MPa]
Maximum tension normal to fibre direction: 50 [MPa]
Maximum compression in fibre direction: 1300 [MPa]
Maximum compression normal to fibre direction: 300 [MPa]
Maximum shear stress: 95 [MPa]
Maximum bonding shear stress: 95 [MPa]

Aluminium honeycomb core, 3/16-5056-.0015, represented as a 3D orthotropic material in MSC.Patran/Nastran [9] and [14]:

The honeycomb specification indicates a cell size of 3/16", and a wall thickness of .0015". FE-analyses on a honeycomb core, and reference [14] are used to provide appropriate values:

Modulus of elastisity in L-direction (ref. Fig. E.2): E_{11} = 0.8 [GPa]
Modulus of elastisity in W-direction (ref. Fig. E.2): E_{22} = 0.7 [GPa]
Modulus of elastisity in T-direction (ref. Fig. E.2): E_{33} = 1.9 [GPa]
Shear modulus: G_{12} = 0.1 [GPa]
Shear modulus: G_{23} = 0.186 [GPa]
Shear modulus: G_{13} = 0.469 [GPa]
Density: ρ = 70.5 [kg/m^3]
CTE: α = 24.0 E-6 [/°C]

Panel lay up:

Antenna (The carbon composite material contains 60% fibre and 40% matrix):

Layer	Material	Thickness (mm)	Fibre angel
1	Carbon composite	0.25	0
2	Carbon composite	0.25	+90
3	Carbon composite	0.25	0
4	Carbon composite	0.25	+90
5	Aluminium honeycomb core	28.0	0
6	Carbon composite	0.25	0
7	Carbon composite	0.25	+90
8	Carbon composite	0.25	0
9	Carbon composite	0.25	+90

Table C.1 Antenna panel layup.

All other panels:

Layer	Material	Thickness (mm)
1	Aluminium skin	1.0
2	Aluminium honeycomb core	18.0
3	Aluminium skin	1.0

Table C.2 Aluminium skin structure panel layup.

D DATA FOR THERMAL MODEL

[9] and [10]:
Heat conductivity for Al 5056 H38 (Core): $k_{Al} = 112$ [W/(m °C)]
Heat capacity for Al 5056 H38 (Core): $C_{Al} = 904$ [J/(kg °C)]
Density for Al 5056 H38 honeycomb core: $\rho = 70.5$ [kg/m^3]
Heat conductivity for Al 6061-T6 (Skin): $k_{Al} = 167$ [W/(m °C)]
Heat capacity for Al 6061-T6 (Skin): $C_{Al} = 896$ [J/(kg °C)]
Density for Al 6061-T6 (Skin): $\rho = 2700$ [kg/m^3]

Heat conductivity for antenna copper layer: $k_{Cu} = 390$ [W/(m °C)]
Heat capacity for antenna copper layer: $C_{Cu} = 390$ [J/(kg °C)]
Density for antenna copper layer: $\rho = 8960$ [kg/m^3]

[9], [11] and [12]:
Heat conductivity for T-300 carbon fibre in fibre direction: $k_{f11} = 83.7$ [W/(m °C)]
Heat conductivity for T-300 carbon fibre across fibre direction: $k_{f22} = 8.4$ [W/(m °C)]

Heat capacity for T-300arbon fibre: $C_f = 711$ [J/(kg °C)]
Density for T-300arbon fibre: $\rho = 1772$ [kg/m^3]
Heat conductivity for matrix: $k_m = 0.23$ [W/(m °C)]
Heat capacity for matrix: $C_m = 1575$ [J/(kg °C)]
Density for matrix: $\rho = 1266$ [kg/m^3]

The total heat conductivity in the plane of the honeycomb panels, given the lay up in table C.1 and C.2, is calculated from equations E.5-7 (ref. App. E). Averaged for any direction in the plane, this gives:

Heat conductivity for complete aluminium skin/core body panels: k = 17.7 [W/(m °C)]
Heat conductivity for antenna carbon fibre composite skin only: k = 25.4 [W/(m °C)]

The heat capacity of the complete aluminium skin/core body panels and the antenna carbon fibre composite skin is calculated given the lay up in table C.1 and C.2, and the listed values for heat capacity. This gives:

Heat capacity for antenna carbon fibre composite skin only: $C_{ant} = 990$ [J/(kg °C)]
Heat capacity for complete aluminium skin/core body panel: $C_{ant} = 898$ [J/(kg °C)]

The heat conductivity in the plane of the antenna Kevlar layer, given a symmetric layup with 60% fibre and 40% matrix, is calculated from equations E.5-7 (ref. App. E). Averaged for any direction in the plane, this gives:

Heat conductivity for antenna Kevlar layer, in plane: $k_{K\_in} = 0.0879$ [W/(m °C)]

The heat conductivity through the plane of the antenna Kevlar layer, with 60% fibre and 40% matrix, is calculated from equation E.4 (ref. App. E). This gives:

Heat conductivity for antenna Kevlar layer, through plane: $k_{K\_thr} = 0.0597$ [W/(m °C)]

Heat capacity for antenna Kevlar layer: $C_{Kv} = 834$ [J/(kg °C)]
Density for antenna Kevlar layer: $\rho = 1370$ [kg/m^3]

Thermal Conductances:

The values are given from Terma AS [19], or found in the literature [7]. The conductance at mechanical interfaces depends on several factors such as contact area, surface finish, number of bolts, bolt sizes, bolt torque, interface fillers, isolating shims/spacers. In this FE-model the only contact at the mechanical interfaces are through the bolts. The bolt conductances are adjusted to consider the overall heat transfer at the interface.

For layers of glue, the conductance is calculated from the equation:

Thermal conductance of link:
$$G_{link} = \frac{k_{glue} \cdot A_{glue}}{t_{glue} \cdot n_{link}} \qquad (D.1)$$

- G_{link} = Conductance of link
- k_{glue} = Conductivity of glue
- A_{glue} = Area of glued section
- t_{glue} = Thickness of glue layer
- n_{link} = Number of links

Patches to Kevlar layer glue (4224 links):	0.039	[W/K] per link
Kevlar layer to antenna panel glue (4224 links):	0.0008162	[W/K] per link
Antenna panel to bracket connections (10 links):	0.1	[W/K] per link
Bracket to spacer connections (6 links):	0.1	[W/K] per link
Spacer to mounting ring connections (6 links):	0.1	[W/K] per link
Radiator to star tracker cover connections (2 links):	4.0	[W/K] per link
Star tracker cover to star tracker flange connection (1 link):	0.2	[W/K] per link
Star tracker flange to star tracker lens connection (1 link):	0.1	[W/K] per link
Star tracker flange to mounting ring connections (4 links):	0.36	[W/K] per link
Mounting ring to baffle connections (6 links):	0.00267	[W/K] per link
Antenna to satellite body connections (128 links):	0.0031	[W/K] per link
Large solar panel (-z) to satellite body connections (16 links):	0.01	[W/K] per link
Small solar panel (-y) to satellite body connections (14 links):	0.01	[W/K] per link
Structural side panels (± y and ± z) connections (64 links):	1.0	[W/K] per link
Deck 1 to side panels connections (128 links):	1.1	[W/K] per link
Deck 2 to side panels connections (128 links):	1.1	[W/K] per link
CEU to deck 1 connections (18links):	0.3	[W/K] per link
Momentum wheels 1 and 2 connections (4 links per wheel):	0.75	[W/K] per link
Momentum wheels 3 and 4 connections (4 links per wheel):	0.3	[W/K] per link
Battery to deck 1 connections (10links):	2.0	[W/K] per link
Payload to deck 2 connections (links):	0.2	[W/K] per link
GPS to deck 2 connections (12 links):	0.1	[W/K] per link
Magnetometer to deck 2 connections (10 links):	0.1	[W/K] per link

E THERMAL MODELLING OF HONEYCOMB SANDWICH PANELS

Parameters:

- q - heat-transfer rate
- k - thermal conductivity
- T - temperature
- x - distance in the heat-flow direction
- R_{tot} - Total resistance
- t - Thickness of skin/core

CONDUCTION IN SANDWICH PANELS [16]:

Given Fourier's law: $$q = -kA\frac{\delta T}{\delta x} \qquad \text{(E.1)}$$

According to fig. E.1, integration gives: $$q = \frac{T_1 - T_4}{\frac{\Delta x_A}{k_A A} + \frac{\Delta x_B}{k_B A} + \frac{\Delta x_C}{k_C A}} \qquad \text{(E.2)}$$

Hence we got an analogy to Ohm's law, where the heat-transfer rate is the flow, the temperature difference is the potential, and the combination of thermal conductivity, material thickness and area, represents the resistance.

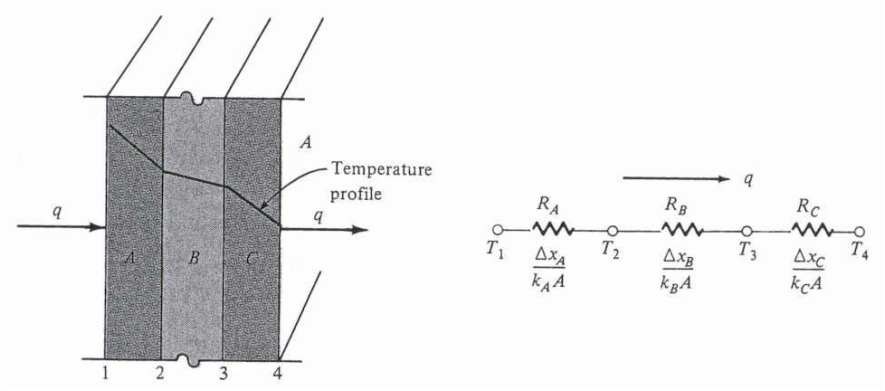

Figure E.1 One-dimensional heat transfer and electrical analogy.

Equation E.2 can be written: $$q = \frac{\Delta T_{total}}{R_{tot}} \qquad \text{(E.3)}$$

Conduction through the panel:
The thermal resistances are put in series, using the electric analogy, which gives:

$$\frac{1}{k_{tot}} = \frac{t_A}{k_A \cdot t_{tot}} + \frac{t_B}{k_B \cdot t_{tot}} + \frac{t_C}{k_C \cdot t_{tot}} \qquad \text{(E.4)}$$

Conduction in the panel plane:
The thermal resistances are put in parallel, using the electric analogy, which gives:

$$k_{tot} = k_A \frac{t_A}{t_{tot}} + k_B \frac{t_B}{t_{tot}} + k_C \frac{t_C}{t_{tot}} \qquad \text{(E.5)}$$

Conduction in a honeycomb core [7]:

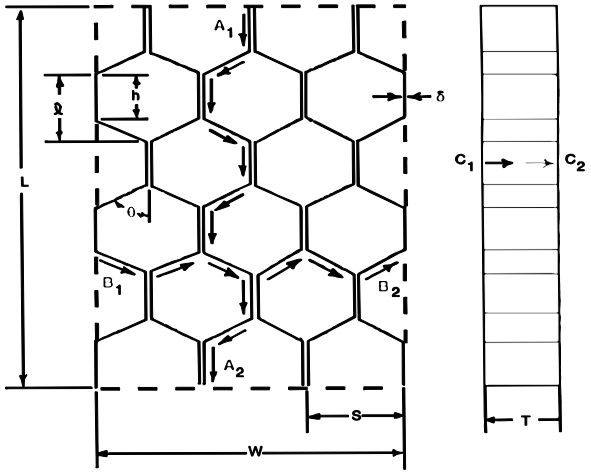

Figure E.2 Core definition.

L - Length of panel
W - Width of panel
T - Thickness of panel
δ - Ribbon thickness
σ - 2h/l = 4/3 for normal hexagonal structure
s, h, l and θ, are given by figure E.2.

CONDUCTIVITY IN L-DIRECTION:

$$k_L = \frac{2k \cdot \delta}{\sigma \cdot s} \tag{E.6}$$

CONDUCTIVITY IN W-DIRECTION:

$$k_W = \frac{k \cdot \delta}{s} \tag{E.7}$$

CONDUCTIVITY IN T-DIRECTION:

$$k_T = \frac{8k \cdot \delta}{3s} \tag{E.8}$$

References

(1) T Eriksen, B Narheim, G Høye, and T Wahl (2001): New micro-satellite based concept for monitoring of maritime traffic by navigation radar detection, in Proceedings of the 8th International symposium on Remote Sensing, volume 4540: Sensors, Systems, and Next Generation Satellites V, pp 166-175, France 17-21 Sept.

(2) SAGSVEEN Bendik Andreas (2001): MECHANICAL AND THERMAL DESIGN CONSIDERATIONS OF THE NSAT-1 MICRO SATELLITE, FFIFv/02933, Unclassified

(3) Terma AS (2002): Phase B Accommodation and Mechanical Requirements Specification, NSAT-1 Star tracker.

(4) Hexcel (1989): TSB 124, Bonded Honeycomb Sandwich Construction, Dublin, California 94568.

(5) Arianespace (May 2000): ASAP 5, User's Manual, Issue 1, Revision 0, Evry Cedex, France, Chapter 3, 4 and 6.

(6) Isaac M. Daniel and Ori Ishai (1994): Engineering Mechanics of Composite Materials, Oxford University Press, New York, Oxford, Chapter 6.3

(7) David G. Gilmore (1994): Satellite thermal control handbook, Aerospace Corporation Press, El Segundo, Calif, Chapter 2, 4, 5 and Appendix.

(8) Vincent L. Pisacane and Robert C. Moore (1994): Fundamentals of Space Systems, Oxford University Press, New York Oxford, page 433.

(9) www.matweb.com.

(10) Aylward & Findlay (1974): SI chemical data, 2nd edition, JOHN WILEY & SONS, Park road, Milton, Qld 4064, 6.

(11) P.L.N Murthy, C.A Gynty, J.G Sanfeliz (des. 1991): Second generation Integrated Composite Analyser, ICAN, Appendix B: Dedicated Data Bank, NASA Lewis Research Centre, Cleveland Ohio.

(12) Anand V. Rau, Ph.D (2002): Shadé Inc. 5049 Russell Circle, Lincoln, NE 68506.

(13) C.Thaulow, S.Støren, C.G.Gustafson, E.Bardal, R.Birkeland, J.H.Ulvensøen (1996-1997): 62144 Materialteknikk, Bind 2, NTNU, Institutt for Maskinkonstruksjon og Materialteknikk, Trondheim, Norway, Chapter 11.

(14) Hexcel (1989): TSB 124, Bonded Honeycomb Sandwich Construction, Dublin, California 94568.

(15) B. Sagsveen (2003): bas$ on 'hbi-fil' (Z:) /satellitt/faseB> "bbq_multipanel_albedo.xls" and "bbq_multipanel_ir.xls".

(16) J.P Holmann (1990): Heat Transfer, McGraw-Hill, Inc., USA, 27-30.

(17) COI (Composite Optics Inc.), San Diego, CA 92121 (2002): NSAT-1 Antenna System Trade Study, Final Presentation for Ericsson A/S.

(18) Minutes of the meeting: Ericsson midway reporting, Status meeting, Kjeller, Norway, Sept. 4th, 2002.

(19) Jan Kjær Sørensen, Terma AS (2002): Private communication.

(20) Terma AS: Meeting report, NSAT-1 Phase B Final Presentation, Birkerød, Denmark, Oct. 31st. to Nov.1st, 2002.

List of acronyms and abbreviations

ASAP 5	Ariane Structure for Auxiliary Payload 5
BOL	Beginning Of Life
BTU	British Thermal Unit
CAD	Computer Aided Design
CEU	Central Electronics Unit
CTE	Coefficient of Thermal Expansion
EOL	End Of Life
FEM	Finite Element Method
FFI	Forsvarets forskningsinstitutt (Norwegian Defence Research Establishment)
IR	Infra Red
MSC	The MacNeal-Schwendler Corporation
NSAT-1	Norwegian micro-satellite no.1

DISTRIBUTION LIST

FFIFv **Dato:** 21. februar 2003

RAPPORTTYPE (KRYSS AV)	RAPPORT NR.	REFERANSE	RAPPORTENS DATO
X RAPP ☐ NOTAT ☐ RR	2003/01407	FFIFv/83401/924	21. februar 2003
RAPPORTENS BESKYTTELSESGRAD		ANTALL TRYKTE UTSTEDT	ANTALL SIDER
Unclassified		54	70
RAPPORTENS TITTEL		FORFATTER(E)	
THERMAL AND MECHANICAL ANALYSES FOR THE NSAT-1 PHASE B STUDY		SAGSVEEN Bendik Andreas	
FORDELING GODKJENT AV UNDERDIREKTØR		FORDELING GODKJENT AV AVDELINGSSJEF:	
Bjørn Bergersen		Svein Rollvik	

EKSTERN FORDELING

ANTALL	EKS NR	TIL
1		FO/E v/ Udir Magne Thunestvedt
1		FO/E v/ Oing Runar Jørgensen
1		FOHK v/ KK Kjetil Utne
1		LDKN v/ OK Egil Vasstrand
1		FO/FST v/ KK Rolf M Stein
1		FO/FST v/ Oblt Gaute Dyrdal
1		Ericsson AS v/ Jens Hjelmstad
1		Terma AS v/ Jan Kjær Sørensen, Aerospace division, DK-8520 Lystrup, Denmark

INTERN FORDELING

ANTALL	EKS NR	TIL
14		FFI-Bibl
1		FFI-ledelse
1		FFIE
1		FFISYS
1		FFIBM
1		FFIN
3		FFIFV
10		Forfattereksemplar(er)
1		Bjørn Narheim, FFIE
1		Gudrun Høye, FFIE
1		Torkild Eriksen, FFIE
1		Vegard Arneson, FFIE
1		Bente J Meland, FFIE
1		Hans Øhra, FFIE
1		Morten Mjanger, FFIE
1		Jan Hammerstad, FFIE
1		Vidar S Andersen, FFIE
1		Bendik Sagsveen, FV
1		Jan Rune Nilssen, FV
1		Bjørn Bergersen, FV
1		Bendik Sagsveen, FV
1		Tor Alexander Fjeldly, BM
		ELEKTRONISK FORDELING:
		Terje Wahl, FFISYS
		FFI-veven